PHYSICAL REVIEW B **78**, 245121 (2008)

Perturbative approach to an exactly solved problem: Kitaev honeycomb model

Julien Vidal,[1,*] Kai Phillip Schmidt,[2,†] and Sébastien Dusuel[3,‡]
[1]*Laboratoire de Physique Théorique de la Matière Condensée, CNRS UMR 7600, Université Pierre et Marie Curie (Paris 06), 4 Place Jussieu, 75252 Paris Cedex 05, France*
[2]*Lehrstuhl für theoretische Physik, Otto-Hahn-Straße 4, D-44221 Dortmund, Germany*
[3]*Lycée Saint-Louis, 44 Boulevard Saint-Michel, 75006 Paris, France*
(Received 9 September 2008; published 29 December 2008)

We analyze the gapped phase of the Kitaev honeycomb model perturbatively in the isolated-dimer limit. Our analysis is based on the continuous unitary transformations method, which allows one to compute the spectrum as well as matrix elements of operators between eigenstates at high order. The starting point of our study consists of an exact mapping of the original honeycomb spin system onto a square-lattice model involving an effective spin and a hard-core boson. We then derive the low-energy effective Hamiltonian up to order 10 which is found to describe an interacting-anyon system, contrary to the order 4 result which predicts a free theory. These results give the ground-state energy in any vortex sector and thus also the vortex gap, which is relevant for experiments. Furthermore, we show that the elementary excitations are emerging free fermions composed of a hard-core boson with an attached spin- and phase-operator string. We also focus on observables and compute, in particular, the spin-spin correlation functions. We show that they admit a multiplaquette expansion that we derive up to order 6. Finally, we study the creation and manipulation of anyons with local operators, show that they also create fermions, and discuss the relevance of our findings for experiments in optical lattices.

DOI: 10.1103/PhysRevB.78.245121 PACS number(s): 75.10.Jm, 03.65.Vf, 05.30.Pr

I. INTRODUCTION

Elementary particles can be classified in two categories according to the value of their spin. Half-integer spin particles obey Fermi-Dirac statistics and are called fermions, whereas integer-spin particles obey Bose-Einstein statistics and are known as bosons. However, some quantum objects may obey other (fractional) statistics describing nontrivial braiding as initially suggested by Leinaas and Myrheim[1] more than 30 years ago and by Wilczek[2,3] in the 1980s. Despite numerous theoretical works, these so-called anyons are still waiting for a direct observation although recent experimental proposals are very promising (see Ref. 4).

In the last years, anyons have drawn much attention because of their interest for topological quantum computation.[5] In this perspective, several models have been proposed, among which the celebrated toric code,[6] which is a spin-1/2 system whose elementary excitations behave as semions. However, the experimental realization of this system is rather tricky since it involves four-spin interactions. Here, we shall focus on another system originally proposed by Kitaev,[7] which only involves two-spin interactions. This model is very rich since it contains Abelian and non-Abelian anyonic as well as fermionic excitations. Thus, it has been the subject of many recent studies concerning the spectrum,[8–16] the correlation functions and the entanglement,[16–20] or the quench dynamics.[21,22] Let us also mention several extensions,[23–25] among which the analysis of time-reversal symmetry-breaking terms,[26,27] which may give rise to a chiral spin liquid.

Furthermore, this model is susceptible to be realized in various experimental systems such as polar molecules, ultracold atoms,[28–31] or Josephson junctions.[32] It thus constitutes an appealing candidate for the observation of anyons. Nevertheless, the presence of fermions in the spectrum may spoil the detection process; a point completely missed in a recent proposal (see Ref. 33 for explanation and Ref. 16 for details).

The goal of the present paper is to investigate the gapped phase of the Kitaev honeycomb model.[7] Indeed, in his remarkable seminal paper, Kitaev[6,7] mainly focused on the special subspace of the Hilbert space to which the ground state belongs to and the low-energy spectrum of other subspaces has only been discussed lately.[13] Our aim is to bridge this gap by providing a high-order perturbative analysis, in the isolated-dimer limit, of the spectrum as well as some interesting results about the creation and the manipulation of anyons, which is of relevance for experiments.[30,31] Part of our results have already been given in two short papers,[13,16] and the present paper may be considered as an extended and detailed version of these works. However many other results are presented here, among which the interplay between fermions and anyons under string operations discussed in Sec. IX.

This paper is organized as follows. In Sec. II, we introduce the model as well as its main properties. In particular, we discuss the importance of the boundary conditions and insist on the role played by conserved quantities[15] and the constraints resulting from them. In Sec. III, we show how to map the Kitaev model[6,7] involving spins on the honeycomb lattice onto an effective spin and hard-core boson on a square lattice. This mapping is the starting point of the perturbation theory presented in this work. In Sec. IV, we explain how to diagonalize the Hamiltonian order by order using the perturbative continuous unitary transformation (PCUT) method. The study of the low-energy [zero-quasiparticle (0-QP)] sector is the subject of Sec. V, a large part of which is devoted to a pictorial (and hopefully pedagogical) analysis and construction of the eigenstates of the toric code model, which

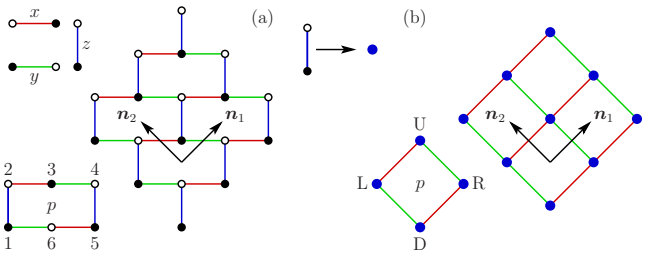

FIG. 1. (Color online) Mapping of the honeycomb (brick-wall) lattice onto a square lattice with unit basis vectors $\boldsymbol{n}_1$ and $\boldsymbol{n}_2$. Each z dimer with four-spin configurations is replaced by a single site with 4 degrees of freedom: the occupation number of hard-core boson (0 or 1) and the effective spin ($\Uparrow$, or $\Downarrow$), which is chosen as the spin of the black site of the considered z dimer. The numbering of the sites of a plaquette p is shown in both cases.

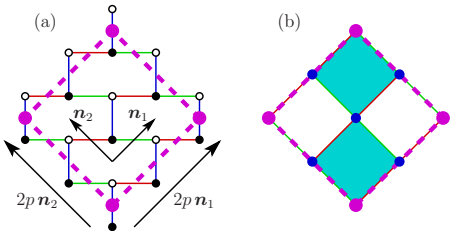

FIG. 2. (Color online) The periodic boundary conditions used in this work (a) on the original brick-wall lattice and (b) on the effective square lattice of z dimers (see Fig. 1). In the figure $p=1$. In both cases, the finite-size system is put on a torus obtained by identifying the opposite sides of the dashed (magenta) square. For clarity, the site at the point chosen as the origin has been depicted bigger. Half the square plaquettes in (b) have been colored in cyan (gray) to show that the periodic boundary conditions allow us to bicolor the lattice.

naturally emerges from this problem. There, we give the perturbative expansion form of the ground-state energy for any vortex configuration. The effective low-energy theory is found to be described by interacting anyons contrary to the lowest-order result which predicts free anyons.[7] Section VI focuses on the study of the one-quasiparticle (1-QP) subspace, where the physics is shown to be that of a particle hopping in a magnetic field with zero or half a flux quantum per elementary plaquette. The demonstration of the fermionic nature (known from exact solutions) of the quasiparticles is briefly sketched in Sec. VII. In Sec. VIII, we provide some checks of our results by analyzing simple vortex configurations, which allow for an exact solution. The spin-spin correlation functions and the manipulation of anyons are tackled in Sec. IX, which is devoted to the renormalization of observables. Finally, we discuss several issues and give some perspectives. Technical details as well as all relevant coefficients involved in the perturbative expansions are gathered in Appendixes A–F.

In what follows, we tried to be as pedagogical as possible and always favored simple demonstrations on concrete examples rather than lengthy proofs for general situations. We hope that it will help the reader to understand the richness of this model.

II. MODEL

A. Hamiltonian and boundary conditions

The model considered in this work is a spin-1/2 system proposed by Kitaev[7] in which spins are located at the vertices of a honeycomb lattice. Since the honeycomb lattice is topologically equivalent to the brick-wall lattice, we shall always represent it as shown in Fig. 1(a). In this lattice, one distinguishes three types of links (x, y, and z) to which one associates three different couplings and interactions. The Hamiltonian of the system is

$$H = -\sum_{\alpha=x,y,z}\ \sum_{\alpha\ \text{links}} J_\alpha \sigma_i^\alpha \sigma_j^\alpha, \tag{1}$$

where σ_i^α are the usual Pauli matrices at site i. In the following we assume, without loss of generality,[7] that $J_\alpha \geq 0$ for all α and $J_z \geq J_x, J_y$.

We will either work with an infinite system and open boundary conditions (a plane) or with a finite (or infinite) system and periodic boundary conditions (PBCs) (a torus). In the latter case and for reasons that will become clearer in the following (in particular, see Sec. V B), we shall restrict ourselves to the PBCs depicted in Fig. 2. The number of sites N_s is $N_s = 2(2p)^2 = 8p^2$, with $p \in \mathbb{N}$ [$p=1$ in Fig. 2(a)]. Let us anticipate what follows and mention that these boundary conditions are such that the lattice of z dimers [Fig. 1(b)] can be bicolored as shown in Fig. 2(b).

B. Conserved quantities

A remarkable property of Hamiltonian (1) is that its elementary operators $K_{ij} = \sigma_i^\alpha \sigma_j^\alpha$ commute with plaquette operators W_p so that $[H, W_p] = 0$. For the plaquette p shown in Fig. 1(a), such an operator is defined as

$$W_p = K_{12}K_{23}K_{34}K_{45}K_{56}K_{61} = \sigma_1^x \sigma_2^y \sigma_3^z \sigma_4^x \sigma_5^y \sigma_6^z. \tag{2}$$

Let us mention that in the expression of W_p in terms of the K's, one could have started at any site instead of site 1 and/or one could have taken the product of K's counterclockwise instead of clockwise. Furthermore, the expression in terms of σ's could also be written as $W_p = \Pi_i \sigma_i^{\text{out}(i)}$, where i runs over the set of six spins around the plaquette p and where the notation out(i) means the "outgoing" direction at site i, with respect to the plaquette's contour. An illustration of the W_p operator is given in Fig. 3.

Since $W_p^2 = \mathbb{I}$, the eigenvalues of the plaquette operators are $w_p = \pm 1$. Note that $[W_p, W_{p'}] = 0$, as can be shown from the usual Pauli matrix algebra. As a consequence, H and the W_p's can be diagonalized simultaneously. Following Kitaev,[6,7] we will call a vortex sector a subspace of the Hilbert space with a given map of the w_p's. By definition a vortex is a plaquette for which $w_p = -1$ so that, for example, the vortex-free sector is defined by $w_p = +1$ for all p's.

In fact, all loop operators made of "outgoing spins" (see Figs. 4 and 5) are conserved and all commute with each other, which can be verified in the same way as for the W_p's. However, not all of them can be set independently to ± 1. Some relations among them arise from the following fact

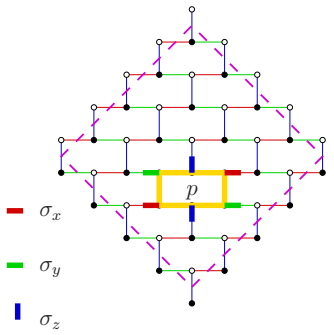

FIG. 3. (Color online) Illustration of the conserved plaquette quantity W_p. The thick yellow (lightest gray) line delimitates the plaquette p. The thick red (gray), green (light gray), or blue (dark gray) segments represent the Pauli matrices $\sigma_i^{\text{out}(i)}$.

(which can be checked by studying all possible cases): the product of W_p and a nearby loop operator $\mathcal{L}$ gives a new loop operator $\mathcal{L}'=W_p\mathcal{L}$, as illustrated on a particular example in Fig. 4.

As an illustration of other relations involving loop operators around the torus, with the loops of Fig. 5, one has

$$\mathcal{L}_a = \prod_{n=1}^{6} W_{a_n}, \tag{3}$$

$$\mathcal{L}_b' = \mathcal{L}_b \prod_{n=1}^{8} W_{b_n}, \tag{4}$$

$$\mathcal{L}_d = -\mathcal{L}_a\mathcal{L}_b\mathcal{L}_c, \tag{5}$$

where we have denoted, for example, $\mathcal{L}_a=\Pi_{i\in\mathcal{C}_a}\sigma_i^{\text{out}(i)}$. The minus sign in the last equation above comes from the crossing of $\mathcal{L}_b$ and $\mathcal{L}_c$. In the three expressions above, the product of plaquette operators could also have been taken over the complementary set of plaquettes. Indeed, on the torus the relations among loop operators yield the following constraint:

$$\prod_{\text{all } p\text{'s}} W_p = \mathbb{I}, \tag{6}$$

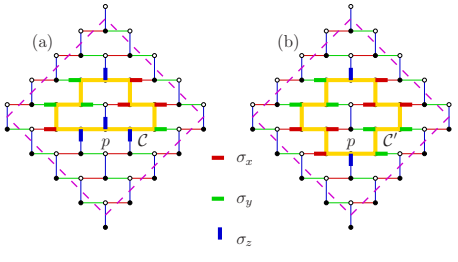

FIG. 4. (Color online) Illustration of the relation $\mathcal{L}'=W_p\mathcal{L}$, with $\mathcal{L}=\Pi_{i\in\mathcal{C}}\sigma_i^{\text{out}(i)}$, W_p already shown in Fig. 3 and $\mathcal{L}'=\Pi_{i\in\mathcal{C}'}\sigma_i^{\text{out}(i)}$. The thick yellow (lightest gray) line in (a) represents the contour $\mathcal{C}$ and the one in (b) represents $\mathcal{C}'$. As in Fig. 3, the thick red (gray), green (light gray), or blue (dark gray) segments represent the Pauli matrices $\sigma_i^{\text{out}(i)}$.

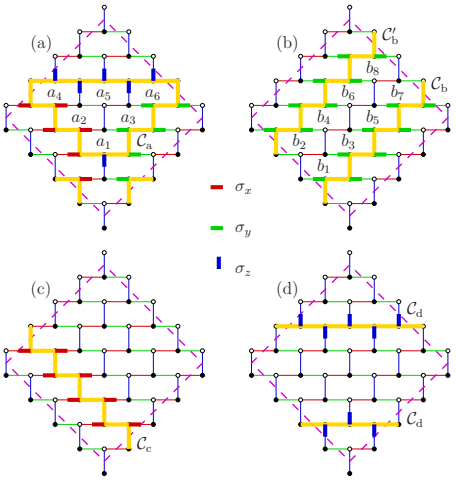

FIG. 5. (Color online) Examples of conserved loop operators $\mathcal{L}=\Pi_{i\in\mathcal{C}}\sigma_i^{\text{out}(i)}$ in a finite-size system with PBC.

showing in particular that *the number of vortices has to be even in a system with PBC*.

From examples shown in Fig. 5, one can deduce that all W_p's [except one, because of Eq. (6)] and $\mathcal{L}_b$ and $\mathcal{L}_c$ can be set independently to ± 1, which then imposes all other conserved quantities.

C. Some results from the exact solution

The above discussed local conserved quantities are not sufficient to fully diagonalize the Hamiltonian. Indeed, if N_s is the number of sites, then there is a total of $N=N_s/2$ plaquettes but only $N-1$-independent ones. With the two cycles around the torus, this gives $N+1$-independent conserved quantities, which are obviously smaller than N_s.

However, H has a crucial property: it can be transformed into a free Majorana fermion Hamiltonian and is, thus, exactly solvable. Let us also mention that another solution based on the Jordan-Wigner transformation maps the spin Hamiltonian H onto a spinless fermions system with p-wave pairing.[9,11,12]

As shown by Kitaev,[7] the ground state of H lies in the vortex-free sector and the phase diagram contains, in this sector, two phases: a gapped phase for $J_z>J_x+J_y$ and a gapless phase for $J_z\leq J_x+J_y$. In the gapped phase the low-energy excitations are Abelian anyons (semions), whereas in the gapless phase, the low-energy excitations are fermionic. The gapless phase acquires a gap in the presence of a magnetic field and then contains gapped non-Abelian anyon excitations. The phase diagram has also been investigated in other vortex configurations such as the vortex-full sector and similar phases have been obtained. More precisely, one has a gapped phase for $J_z^2>J_x^2+J_y^2$ and a gapless phase in the opposite case.[14]

Our goal here is to determine the low-energy spectrum for any vortex configuration. Of course, one may use the fermionic Hamiltonian mentioned above, but it can only be exactly diagonalized for translation-invariant configuration. Here, we follow an alternative route by focusing on the isolated-dimer limit $J_z \gg J_x, J_y$.

III. MAPPING ONTO AN EFFECTIVE-SPIN BOSON PROBLEM

A. Mapping of the Hamiltonian

The very first step of our analysis consists of mapping the four possible states of the two spins of a z dimer onto those of an effective spin and a hard-core boson. More precisely, denoting $|\uparrow\rangle$ ($|\downarrow\rangle$) the eigenstate of σ_z with eigenvalue +1 (−1), an isolated z dimer can be in one of the two low-energy states $\{|\uparrow\uparrow\rangle,|\downarrow\downarrow\rangle\}$ with energy $-J_z$ or in one of the two high-energy states $\{|\uparrow\downarrow\rangle,|\downarrow\uparrow\rangle\}$ with energy $+J_z$. Keeping in mind that our aim is to perform a perturbation theory in the limit $J_z \gg J_x, J_y$, it is natural to interpret the change from a ferromagnetic to an antiferromagnetic configuration as the creation of a particle with an energy cost $2J_z$. By construction, such a particle is a hard-core boson. The remaining degree of freedom can be described by a spin 1/2, indicating which of the two configurations is realized. There are many possible parametrizations but here we choose the following:

$$|\uparrow\uparrow\rangle = |\Uparrow 0\rangle, \quad |\downarrow\downarrow\rangle = |\Downarrow 0\rangle, \quad |\uparrow\downarrow\rangle = |\Uparrow 1\rangle, \quad |\downarrow\uparrow\rangle = |\Downarrow 1\rangle. \tag{7}$$

The left (right) spin is the one of the black (white) site of the dimer ($|\uparrow\downarrow\rangle = |\uparrow_\bullet\downarrow_\circ\rangle$, etc.). Double arrows represent the state of the effective spin, which is the same here as the state of the left (black) spin.

Within such a mapping, effective spins and hard-core bosons live on the effective square lattice of z dimers (see Fig. 1). This lattice is shown again in Fig. 2(b) together with the PBC, which are such that it can be bicolored. In what follows, the sites of the effective lattice will be denoted with bold letters, such as $\boldsymbol{i}$.

Let us now write Hamiltonian (1) in this language. Therefore, we first translate the action of the spin operators in the effective-spin boson (ESB) formalism. It is easy to check that one has

$$\sigma^x_{i,\bullet} = \tau^x_{\boldsymbol{i}}(b^\dagger_{\boldsymbol{i}} + b_{\boldsymbol{i}}), \quad \sigma^x_{i,\circ} = b^\dagger_{\boldsymbol{i}} + b_{\boldsymbol{i}},$$

$$\sigma^y_{i,\bullet} = \tau^y_{\boldsymbol{i}}(b^\dagger_{\boldsymbol{i}} + b_{\boldsymbol{i}}), \quad \sigma^y_{i,\circ} = \mathrm{i}\tau^z_{\boldsymbol{i}}(b^\dagger_{\boldsymbol{i}} - b_{\boldsymbol{i}}),$$

$$\sigma^z_{i,\bullet} = \tau^z_{\boldsymbol{i}}, \quad \sigma^z_{i,\circ} = \tau^z_{\boldsymbol{i}}(1 - 2b^\dagger_{\boldsymbol{i}} b_{\boldsymbol{i}}). \tag{8}$$

The operators $\tau^\alpha_{\boldsymbol{i}}$ ($\alpha = x,y,z$) are the Pauli matrices acting on the effective spin at site $\boldsymbol{i}$, while $b_{\boldsymbol{i}}$ and $b^\dagger_{\boldsymbol{i}}$ are hard-core bosonic annihilation and creation operators, satisfying the usual on-site anticommutation relation $\{b_{\boldsymbol{i}}, b^\dagger_{\boldsymbol{i}}\} = \mathbb{I}$ (and operators on different sites commute). Setting once for all $J_z = 1/2$ so that creating a boson costs an energy 1 in the isolated-dimer limit, Hamiltonian (1) reads

$$H = -\frac{N}{2} + Q + T_0 + T_{+2} + T_{-2}, \tag{9}$$

where N is the number of z dimers (or, equivalently, of square plaquettes), and

$$Q = \sum_{\boldsymbol{i}} b^\dagger_{\boldsymbol{i}} b_{\boldsymbol{i}}, \tag{10}$$

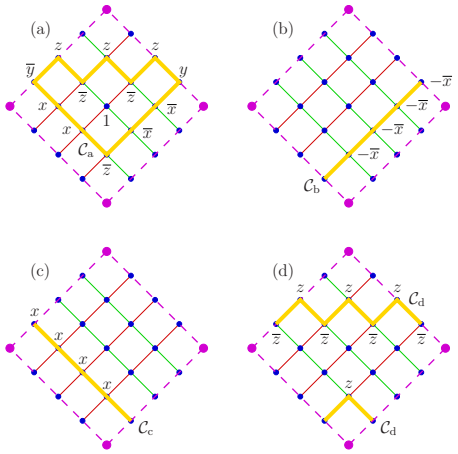

FIG. 6. (Color online) On the four figures, the thick yellow (lightest gray) line represents the contours $\mathcal{C}$. The operators $\omega_{\boldsymbol{i}}$ which are such that the loop operators read $\mathcal{L} = \Pi_{\boldsymbol{i}\in\mathcal{C}}\omega_{\boldsymbol{i}}$ are indicated in the figures. In the present case, they can take the following values $x = \tau^x$, $\bar{x} = (-1)^{b^\dagger b}\tau^x$ (and the same for y and z), and $-\bar{x} = -(-1)^{b^\dagger b}\tau^x$. These figures are the same as the ones of Fig. 5 but on the effective lattice.

$$T_0 = -\sum_{\boldsymbol{i}} (J_x t_{\boldsymbol{i}}^{\boldsymbol{i}+\boldsymbol{n}_1} + J_y t_{\boldsymbol{i}}^{\boldsymbol{i}+\boldsymbol{n}_2} + \mathrm{H.c.}), \tag{11}$$

$$T_{+2} = -\sum_{\boldsymbol{i}} (J_x v_{\boldsymbol{i}}^{\boldsymbol{i}+\boldsymbol{n}_1} + J_y v_{\boldsymbol{i}}^{\boldsymbol{i}+\boldsymbol{n}_2}) = (T_{-2})^\dagger. \tag{12}$$

These operators are built from local hopping and pair-creation operators,

$$t_{\boldsymbol{i}}^{\boldsymbol{i}+\boldsymbol{n}_1} = b^\dagger_{\boldsymbol{i}+\boldsymbol{n}_1} b_{\boldsymbol{i}} \tau^x_{\boldsymbol{i}+\boldsymbol{n}_1}, \quad t_{\boldsymbol{i}}^{\boldsymbol{i}+\boldsymbol{n}_2} = -\mathrm{i} b^\dagger_{\boldsymbol{i}+\boldsymbol{n}_2} b_{\boldsymbol{i}} \tau^y_{\boldsymbol{i}+\boldsymbol{n}_2} \tau^z_{\boldsymbol{i}},$$

$$v_{\boldsymbol{i}}^{\boldsymbol{i}+\boldsymbol{n}_1} = b^\dagger_{\boldsymbol{i}+\boldsymbol{n}_1} b^\dagger_{\boldsymbol{i}} \tau^x_{\boldsymbol{i}+\boldsymbol{n}_1}, \quad v_{\boldsymbol{i}}^{\boldsymbol{i}+\boldsymbol{n}_2} = \mathrm{i} b^\dagger_{\boldsymbol{i}+\boldsymbol{n}_2} b^\dagger_{\boldsymbol{i}} \tau^y_{\boldsymbol{i}+\boldsymbol{n}_2} \tau^z_{\boldsymbol{i}}. \tag{13}$$

We emphasize that the mapping [Eq. (8)] explicitly breaks the symmetry between white and black sites of the original brick-wall lattice. This is responsible for the apparent breaking of symmetry between the $x/\boldsymbol{n}_1$ and $y/\boldsymbol{n}_2$ directions in Eq. (13). However, for all the physically observable results, this symmetry remains intact (see, for example, the series expansion of eigenenergies in Appendix C). Note however that the $\boldsymbol{n}_1 + \boldsymbol{n}_2$ and $\boldsymbol{n}_1 - \boldsymbol{n}_2$ directions are not equivalent, as can be seen from the underlying brick-wall lattice.

B. Conserved quantities

Let us now rephrase the conserved operators discussed in Sec. II B in the effective language. Using the notations depicted in Fig. 1(b), as well as the mapping [Eq. (8)], the plaquette operators transform into

$$W_p = (-1)^{b^\dagger_{\mathrm{L}} b_{\mathrm{L}} + b^\dagger_{\mathrm{D}} b_{\mathrm{D}}} \tau^y_{\mathrm{L}} \tau^z_{\mathrm{U}} \tau^y_{\mathrm{R}} \tau^z_{\mathrm{D}}. \tag{14}$$

Note that $(-1)^{b^\dagger_{\boldsymbol{i}} b_{\boldsymbol{i}}} = 1 - 2b^\dagger_{\boldsymbol{i}} b_{\boldsymbol{i}}$. In the same vein, for the cycles around the torus shown in Figs. 5(b) and 5(c), which are reproduced for the effective lattice in Figs. 6(b) and 6(c), one has $\mathcal{L}_b = \Pi_{\boldsymbol{i}\in\mathcal{C}_b}[-(-1)^{b^\dagger_{\boldsymbol{i}} b_{\boldsymbol{i}}}\tau^x_{\boldsymbol{i}}] = \Pi_{\boldsymbol{i}\in\mathcal{C}_b}[(-1)^{b^\dagger_{\boldsymbol{i}} b_{\boldsymbol{i}}}\tau^x_{\boldsymbol{i}}]$ (since there is

an even number of sites on the contour with the PBC chosen here), as well as $\mathcal{L}_c=\Pi_{i\in\mathcal{C}_c}\tau_i^x$. The expression for $\mathcal{L}_d$ [see Fig. 5(d)], namely, $\mathcal{L}_d=\Pi_{i\in\mathcal{C}_d}\omega_i$, is a bit more complicated, but it should be clear from Fig. 6(d) what the ω_i's are. Finally, for the contour shown in Fig. 6(a) [which is in correspondence with Fig. 5(a)], one has $\Pi_{p\subset\mathcal{C}_a}W_p=\Pi_{i\in\mathcal{C}_a}\omega_i=\mathcal{L}_a$ with the ω_i's indicated in the figure and with $p\subset\mathcal{C}_a$ meaning the plaquettes p enclosed in the contour $\mathcal{C}_a$. With these notations, one can easily check that Eq. (5) still holds.

The elementary hopping and pair-creation operators, namely, t_i^j and v_i^j with $\boldsymbol{i}$ and $\boldsymbol{j}$ nearest neighbors, have a very remarkable property: they all commute with the W_p's as well as with any other loop operator,

$$[t_i^j,W_p]=[v_i^j,W_p]=[t_i^j,\mathcal{L}]=[v_i^j,\mathcal{L}]=0. \tag{15}$$

The original spin problem on the honeycomb lattice is, thus, mapped onto a quadratic hard-core boson problem on an effective square lattice, with conserved plaquette and loop operators. Let us underline that this mapping is exact and just provides an alternative description of the spin problem. The resulting Hamiltonian (9) remains difficult to diagonalize (except, of course, if one remembers that the model can be fermionized) since (i) bosons are hard core which prevents the use of a Bogoliubov transformation and (ii) bosonic and spin degrees of freedom are correlated. The conserved plaquette operators will of course be useful in simplifying and solving the problem as recently underlined in Ref. 15.

IV. PERTURBATION THEORY IN THE GAPPED PHASE

A. Effective Hamiltonian from PCUTs

The starting point of the present perturbation theory is the isolated-dimer limit, namely, $J_x=J_y=0$. In this limit, the spectrum is made of equidistant and degenerate levels separated by an energy gap $\Delta=2J_z=1$. To compute the perturbative spectrum, there are of course several methods among which Green's function formalism initially used by Kitaev.[7] However, if this approach is efficient to obtain the first nontrivial (nonconstant) correction, it becomes tricky to implement at higher orders.

Here, following Ref. 13, we use an alternative approach based on continuous unitary transformations (CUTs) conjointly proposed by Wegner[34] and Głazek and Wilson.[35,36] We refer the interested reader to Ref. 37 for a recent pedagogical introduction. Its perturbative version denoted PCUTs is especially well suited to the problem at hand. This technique is detailed in several works.[38,39] Let us simply mention that the CUT method requires the choice of a generator that drives the flow of the operators. All the results given here have been obtained with the so-called quasiparticle number-conserving generator first proposed by Mielke[40] for finite matrices and generalized to many-body systems by Knetter and Uhrig.[39]

The latter have computed the perturbative expansion for *any* Hamiltonian of the form

$$H=Q+T_{-2}+T_{-1}+T_0+T_{+1}+T_{+2}, \tag{16}$$

provided two hypothesis are satisfied: (i) the unperturbed Hamiltonian Q has an equidistant spectrum bounded from below; (ii) the perturbing Hamiltonian $\Sigma_{n=-2}^{+2}T_n$ is such that $[Q,T_n]=nT_n$.

Clearly, Hamiltonian (9) meets these two criteria (up to a constant term) noting that in the present case, one has $T_{\pm1}=0$. Here, we have included the "small" parameters, namely J_x and J_y, in the definition of the T_n operators, which is not the convention usually adopted in the CUT community.

The CUT method together with the quasiparticle number-conserving generator unitarily transform Hamiltonian (16) into an effective Hamiltonian $H_{\text{eff}}=U^\dagger HU$ commuting with Q, U being a unitary operator. We give the first terms of the expansion up to order 4 in Appendix A. As can be seen in Table I, the number of terms appearing in the perturbative expansion quickly increases with the order. For instance, at order 2, the effective Hamiltonian reads in our case

$$H_{\text{eff}}=-\frac{N}{2}+Q+T_0-\frac{1}{2}T_{-2}T_{+2}+\frac{1}{2}T_{+2}T_{-2}, \tag{17}$$

whereas at order 10, there are more than 10^4 operators to consider.

Writing H_{eff} this way is only the very first part of the job since one next has to (i) determine its action in each subspace of a given QP number q and (ii) diagonalize H_{eff} in each of these subspaces. This is the object of Secs. V–VII: we first study the lowest-energy states ($q=0$ QP), which is the main contribution of our work; then we turn to the $q=1$ QP states and recover the high-energy gap from the QP dispersion; we end by $q\geq2$ QP states, whose properties determine the statistics of the QPs, and we will see that the QPs behave as fermions, which are, furthermore, noninteracting. This fact is at the origin of a tremendous simplification of the effective Hamiltonian. Indeed, we found that H_{eff} can be written, at all orders and in the thermodynamical limit, as

$$H_{\text{eff}}=E_0+\mu Q-\sum_{\{p_1,\ldots,p_n\}}C_{p_1,\ldots,p_n}W_{p_1}\cdots W_{p_n}-\sum_{\{j_1,\ldots j_n\}}D_{j_1,\ldots,j_n}S_{j_1,\ldots,j_n}b_{j_n}^\dagger b_{j_1}. \tag{18}$$

We shall discuss each term in detail in Secs. V–VII, but let us mention that E_0, μ, C's, and D's are coefficients whose series expansions are computed. The S operators are strings of spin operators τ_j^α and of phase factors $(-1)^{b_j^\dagger b_j}$ on the cluster $\{\boldsymbol{j}_1,\ldots,\boldsymbol{j}_n\}$. This very special form of multiparticle terms [remember $(-1)^{b_j^\dagger b_j}=1-2b_j^\dagger b_j$], leading to phase factors and spin strings only, is responsible for the emergence of fermions in the model.

For a finite-size system with PBC, new terms appear in the effective Hamiltonian. They involve loop operators around the torus and appear at a minimal order being the linear size $2p$ of the lattice. Such loop operators are associated to contours as the ones shown in Figs. 5 and 6, namely, $\mathcal{L}_b$, $\mathcal{L}_c$, and $\mathcal{L}_b'$ for the contours $\mathcal{C}_b$, $\mathcal{C}_c$, and $\mathcal{C}_b'$. The presence of such loop operators in the effective Hamiltonian shows

that the eigenstates of the Hamiltonian are also eigenstates of these loop operators. Their effect is to lift the degeneracies between states [which for each energy is at least four in the thermodynamical limit since some of the excitations are Abelian semions and the genus of a torus is 1 (see Ref. 5)]. We shall not dive into the details of such finite-size corrections since our approach allows us to directly tackle with the most interesting thermodynamical limit. However, let us make a remark about a numerical check of this statement for small system sizes. For a torus whose linear size is strictly smaller than 4, the loop operator terms around the torus dominate the expansion over the W_p's, and for a size of 4 both types of terms start contributing at the same order. One should, thus, not be surprised to find a ground state for $p=1$, which is not in the vortex-free sector.[15]

B. Counting of states

Before we turn to a detailed analysis of each QP subspace, let us show that we do not miss any state using simple counting arguments. We have already seen in Sec. II that one has $N+2$ conserved $\mathbb{Z}_2$ quantities (two loop operators and N plaquette operators), with the constraint $\Pi_p W_p = \mathbb{I}$. There is, in fact, one more relation between the W_p's, involving the number of bosons, which reads

$$\prod_{p\in\text{white}} W_p = (-1)^{\Sigma_i b_i^\dagger b_i} = (-1)^Q = \prod_{p\in\text{cyan(gray)}} W_p, \quad (19)$$

showing that the parity of the number of vortices living on white plaquettes (see Fig. 2) has to be the same as the parity of the number of bosons. The last equality simply comes from the previously mentioned constraint [Eq. (6)]. The first equality can be checked using expression (14) of the W_p's. Indeed, for a site $\boldsymbol{i}$ having a white plaquette on its left and another one on its right, the product of the two associated W_p's will give $\tau_{\boldsymbol{i}}^y \times (-1)^{b_{\boldsymbol{i}}^\dagger b_{\boldsymbol{i}}} \tau_{\boldsymbol{i}}^y = (-1)^{b_{\boldsymbol{i}}^\dagger b_{\boldsymbol{i}}}$. In the same way, for a site $\boldsymbol{i}$ having a white plaquette above it and another one under it, the product of the two associated W_p's will give $\tau_{\boldsymbol{i}}^z \times (-1)^{b_{\boldsymbol{i}}^\dagger b_{\boldsymbol{i}}} \tau_{\boldsymbol{i}}^z = (-1)^{b_{\boldsymbol{i}}^\dagger b_{\boldsymbol{i}}}$. Let us note that Eq. (19) has a meaning in the two bases we are working in, the initial one and the unitarily transformed one. Indeed, in the initial basis, the Hamiltonian H commutes with the parity operator $(-1)^Q$; in the rotated basis, H_{eff} commutes with Q.

We, thus, see that in a subspace with a given number of QPs, there are N-independent conserved $\mathbb{Z}_2$ quantities. Thus, N being the number of effective spins $\tau_{\boldsymbol{i}}$, there is no remaining effective-spin degree of freedom once the $\mathbb{Z}_2$ quantities are chosen. As a conclusion, the q-QP subspace has dimension $d_q = 2^N \binom{N}{q}$, with the usual notation for binomial coefficients. This shows that we miss no state since

$$\sum_{q=0}^{N} d_q = 2^N \sum_{q=0}^{N} \binom{N}{q} = 2^{2N} = 2^{N_s}, \quad (20)$$

where N_s is the total number of spins in the brick-wall lattice.

This discussion furthermore sheds light on the fact that in order to compute eigenenergies, a perturbative expansion of the Kitaev model[6,7] (as opposed to exact numerics) is really of interest only in the 0-QP subspace. Indeed, we have just seen that there are N-independent $\mathbb{Z}_2$ conserved quantities. It is, thus, clear that as soon as we will have written down the effective Hamiltonian in the 0-QP subspace, the Hamiltonian will already be diagonal, whatever the vortex configuration, although writing down the eigenstates of the $\mathbb{Z}_2$ quantities in the basis of effective-spin operators still has to be done. However, in the 1-QP subspace, one will have to diagonalize an $N\times N$ matrix (numerically in the case of a nonperiodic vortex configuration), which is identical to what one has to do when solving the problem exactly as Kitaev did.[6,7] For $q\geq 2$, the perturbative expansion looks even more complicated than the exact solution, but this is an artifact since we recover free fermions.

V. EFFECTIVE HAMILTONIAN IN THE 0-QP SUBSPACE

A. Effective Hamiltonian and eigenenergies

In the 0-QP sector and in the thermodynamical limit, the effective Hamiltonian (18) simplifies and reads

$$H_{\text{eff}}|_{q=0} = E_0 - \sum_{\{p_1,\ldots,p_n\}} C_{p_1,\ldots,p_n} W_{p_1} \cdots W_{p_n}, \quad (21)$$

where $\{p_1,\ldots,p_n\}$ denotes a set of n plaquettes and the W_p's are the conserved plaquette operators introduced in Sec. II. Note than when restricted to the 0-QP sector they simplify to $W_p|_{q=0} = \tau_{\text{L}}^y \tau_{\text{U}}^z \tau_{\text{R}}^y \tau_{\text{D}}^z$ [see Eq. (14)].

As mentioned at the end of Sec. IV B, obtaining eigenenergies only requires a minimal amount of work, namely, replacing each W_p by numbers $w_p = \pm 1$ and doing the same with loop operators, without forgetting about the constraints among these quantities. The perturbative expansions of the coefficients E_0 and $C_{p_1,\ldots,p_n}$ are given in Appendix C. Let us note that $\{p_1,\ldots,p_n\}$ does not need to be a linked cluster of plaquettes (as seen for $C_{p,p+2n_1}$ that is nonvanishing at order 10) and that translational invariance of the Hamiltonian implies that the $C_{p_1,\ldots,p_n}$ coefficients only depend on $n-1$ relative positions of the plaquettes.

The lowest nontrivial order involving the W_p's (order 4) has been derived by Kitaev[7] ($C_p = J_x^2 J_y^2/2$) and led him to identify the effective low-energy theory with the toric code.[6] One of the main results of our work is to show that at order 6 and beyond, one obtains a *multiplaquette expansion* in the effective low-energy Hamiltonian. In other words vortices interact, though they remain static as they have to since the W_p's are conserved. The interaction energies between vortices are not directly the C coefficients. One should write $w_p = 1-2n_p$, where n_p is the number of vortices at plaquette p (0 or 1), then look at coefficients in the expansion in terms of the n_p's. The results of such an analysis for two-vortex interaction energies in the case $J_x = J_y = J$ are illustrated in Fig. 7, which shows that the interaction (i) lowers the energy and is therefore attractive, (ii) is anisotropic even for $J_x = J_y = J$, which is clear from the structure of the underlying brick-wall lattice, and (iii) decreases with the distance d between vortices as expected in a gapped system. Note that for a finite-size system with PBC, the two-vortex configurations with a central vortex and another vortex at one of 1, 5, 6, and 7 sites (see Fig. 7) are forbidden since they violate constraint (19).

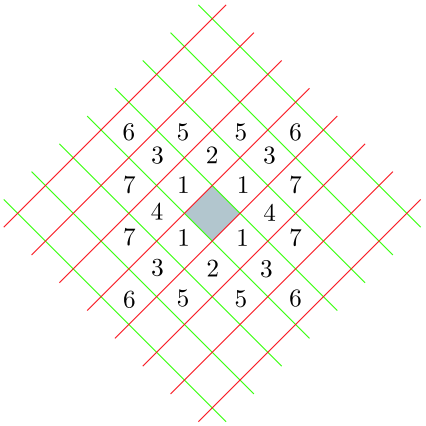

$$\Delta E_{2v}^{(1)} = 2\Delta E_{1v} - \tfrac{7}{2}J^6 - \tfrac{177}{4}J^8 - \tfrac{17831}{32}J^{10}$$
$$\Delta E_{2v}^{(2)} = 2\Delta E_{1v} - \tfrac{165}{4}J^8 - 572J^{10}$$
$$\Delta E_{2v}^{(3)} = 2\Delta E_{1v} - \tfrac{33}{4}J^8 - \tfrac{1001}{8}J^{10}$$
$$\Delta E_{2v}^{(4)} = 2\Delta E_{1v} - \tfrac{11}{4}J^8 - 68J^{10}$$
$$\Delta E_{2v}^{(5)} = 2\Delta E_{1v} - \tfrac{2145}{8}J^{10}$$
$$\Delta E_{2v}^{(6)} = 2\Delta E_{1v} - \tfrac{715}{32}J^{10}$$
$$\Delta E_{2v}^{(7)} = 2\Delta E_{1v} - \tfrac{33}{8}J^{10}$$

FIG. 7. (Color online) Two-anyon configurations (gray central plaquette and one of the numbered plaquettes) on a vortex-free background. ΔE_{1v} (ΔE_{2v}) is the energy cost (at order 10) for adding one vortex (two vortices) to the vortex-free state. ΔE_{1v} reads $\Delta E_{1v}=J^4+8J^6+75J^8+784J^{10}$. For simplicity, we have set here $J_x=J_y=J$ but the results, in the general case, are easily obtained from the coefficients given in Appendix C.

A one-vortex configuration is also forbidden since it violates constraint (6). These configurations would be allowed in an infinite system or in a finite system with open boundary conditions.

A most remarkable point which emerges from the analysis of $H_{\text{eff}}|_0$ is that its eigenstates are those of the W_p's. They are, thus, the same at any order (≥ 4) and are those of the toric code,[6] although their eigenenergy changes with the perturbation order (we emphasize that we are talking about eigenstates of $H_{\text{eff}}|_0$ and not of the original Hamiltonian H). We graphically sketch the construction of these eigenstates in Sec. V B, which will also prove to be useful for the ($q \geq 1$) QP sectors, and show explicitly that they obey anyonic, more precisely semionic, statistics. Our discussion of the toric code focuses on peculiarities related to our way of studying the problem that is not restricted to the 0-QP subspace. For more details about the toric code model, we refer the interested reader to Refs. 5–7.

B. Toric code in a nutshell

1. Mapping to the toric code

As we have seen in Secs. II–IV, the eigenstates of the effective Hamiltonian in the 0-QP subspace are the eigenstates of the W_p's and of the $\mathcal{L}$'s. We recall that in this subspace, the plaquette operators read $W_p|_{q=0}=\tau_{\text{L}}^y\tau_{\text{U}}^z\tau_{\text{R}}^y\tau_{\text{D}}^z$ [see Eq. (14) and Fig. 1(b)]. A similar simplification occurs for the $\mathcal{L}$'s. As mentioned by Kitaev[7] (for the Hamiltonian at order 4), the effective Hamiltonian could be studied directly, but it is much easier to visualize the eigenstates by performing some spin rotations and bring the Hamiltonian to the one of the toric code (generalized by multivortex terms). Thanks to the special PBC we have chosen, the lattice sites can be bicolored as illustrated in Fig. 8. Then, one performs a different rotation on the two kinds of sites,

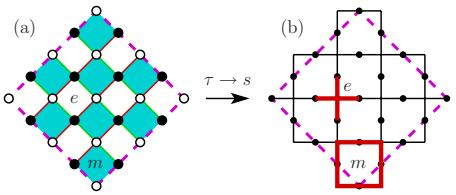

FIG. 8. (Color online) Illustration of the two different points of view one can have of a bicolored lattice: sites are at vertices in (a) and on the bonds in (b). The plaquette m in (a) remains a plaquette in (b), while the plaquette operator e transforms into a star operator.

$$\tau_{\bullet}^x = s^y, \quad \tau_{\bullet}^y = s^z, \quad \tau_{\bullet}^z = s^x,$$
$$\tau_{\circ}^x = -s^y, \quad \tau_{\circ}^y = s^x, \quad \tau_{\circ}^z = s^z. \tag{22}$$

This way, a cyan (gray) (respectively, white) plaquette such as m (respectively, e) in Fig. 8(a) transforms into a plaquette (star) term $B_m=(-1)^{b_{\text{L}}^\dagger b_{\text{L}}+b_{\text{D}}^\dagger b_{\text{D}}}s_{\text{L}}^z s_{\text{U}}^z s_{\text{R}}^z s_{\text{D}}^z$ (respectively, $A_e=(-1)^{b_{\text{L}}^\dagger b_{\text{L}}+b_{\text{D}}^\dagger b_{\text{D}}}s_{\text{L}}^x s_{\text{U}}^x s_{\text{R}}^x s_{\text{D}}^x$), as shown with thick (red) lines in Fig. 8(b). We have kept track of the phases involving boson numbers because our construction will be needed for ($q \geq 1$) subspaces, but it is clear that they can be dropped *in the 0-QP subspace*. Let us mention that the distinction between plaquette and star terms is purely conventional. The letters m and e refer to the magnetic and electric vocabulary also used by Kitaev,[7] although we emphasize there is absolutely no difference between an A and a B operator, which are both disguised W operators. Up to an additive constant term, the effective Hamiltonian in the 0-QP subspace, and at order 4, finally reads (with $J_{\text{eff}}=J_x^2J_y^2/2$)

$$H_{\text{eff}}|_{q=0} = -J_{\text{eff}}\left(\sum_e A_e + \sum_m B_m\right). \tag{23}$$

We work with this lowest (nontrivial) order Hamiltonian because the eigenstates of $H_{\text{eff}}|_{q=0}$ remain the same whatever the order in perturbation. One should simply remember that the eigenstates of H also have to be eigenstates of $\mathcal{L}$ operators. If the PBC is not of the type we use (see Fig. 2), the sites can usually not be bicolored and the rotations [Eq. (22)] cannot be performed, which makes the construction much more complicated, and we shall refer the interested readers to Ref. 41.

2. Construction of the ground state(s)

As a warm up, let us construct a ground state of $H_{\text{eff}}|_0$, i.e., an eigenstate of all B_m and A_e operators with eigenvalue 1 (there are actually four of these). An eigenstate of all B_m's is, for example, the "reference" state $|\Uparrow\rangle$ where all spins s point in the $+z$ direction, such that for all $\boldsymbol{i}$ one has

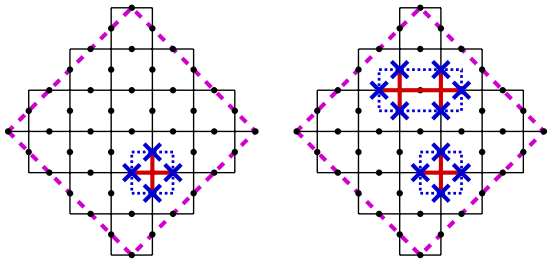

FIG. 9. (Color online) Two of the states entering the equal-weight superposition in Eq. (24). Crosses on the sites indicate a spin flip with respect to the reference state $|\Uparrow\rangle$, where all spins point upward (the A_e operators are still pictured by thick crosses at the vertices). The loops, in dotted lines, are obtained by joining the flipped spins.

$s_i^z|\Uparrow\rangle=|\Uparrow\rangle$. This state is not an eigenstate of the A_e operators yet, but a simple projection yields the desired state,

$$2^{N/4-1/2}\prod_e\left(\frac{\mathbb{I}+A_e}{2}\right)|\Uparrow\rangle\otimes|0\rangle_b, \tag{24}$$

whose normalization follows from the number $N/2$ of e's and the property $\Pi_e A_e=\mathbb{I}$ [see Eq. (19)]. The state $|0\rangle_b$ indicates that there is no quasiparticle, i.e., no hard-core boson. A graphical interpretation can be given of state (24): it is an equal-weight superposition of multiloop configurations produced by the A_e operators, as the ones shown in Fig. 9.

One next has to get an eigenstate of two independent loop operators, which we choose to be $\mathcal{L}_b$ and $\mathcal{L}_c$ (see Figs. 5 and 6) and, which, from now on, will be denoted $\mathcal{L}^x$ and $\mathcal{L}^y$, with eigenvalues l^x and l^y. The expressions of these operators in the s-spin language are given in Fig. 10.

Note that in the 0-QP subspace, one could also have used other conserved loop operators, which are products of s^x or of s^z on the contours defining $\mathcal{L}^x$ and $\mathcal{L}^y$. Such operators resemble more the ones used by Kitaev,[6] but they are conserved only in the 0-QP subspace (in contrast to $\mathcal{L}^x$ and $\mathcal{L}^y$), and so will not prove to be very useful in the following.

As can be seen in Fig. 10, $\mathcal{L}_x$ and $\mathcal{L}_y$ perform spin flips, with respect to $|\Uparrow\rangle$ on their associated contours. The four ground states of Eq. (23) are then obtained with another projection and proper normalization,

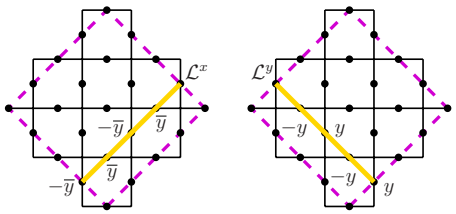

FIG. 10. (Color online) The two loop operators $\mathcal{L}^x$ and $\mathcal{L}^y$ and their contours in yellow (lightest gray) thick lines, corresponding to $\mathcal{C}_b$ and $\mathcal{C}_c$ in Fig. 6. As in the latter figure, but for s spins instead of τ spins, y means s^y, etc. In the 0-QP sector, $\bar{y}=(-1)^{b^\dagger b}s^y$ is the same as y.

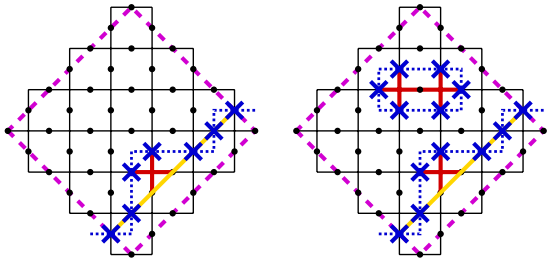

FIG. 11. (Color online) Two of the states entering the equal-weight (in absolute value) superposition in Eq. (25), involving the $\mathcal{L}^x$ loop operator. Graphical conventions are the same as in Figs. 9 and 10.

$$|\{w_p=1\},l^x,l^y\rangle_0=2^{N/4+1/2}\left(\frac{\mathbb{I}+l^x\mathcal{L}^x}{2}\right)\left(\frac{\mathbb{I}+l^y\mathcal{L}^y}{2}\right)\times\prod_e\left(\frac{\mathbb{I}+A_e}{2}\right)|\Uparrow\rangle\otimes|0\rangle_b. \tag{25}$$

These four states are equal-weight (in absolute value) superposition of all possible multiloop configurations, produced by the A_e operators as in Fig. 9, as well as the $\mathcal{L}^x$ and $\mathcal{L}^y$ operators, as illustrated in Fig. 11 for $\mathcal{L}^x$.

Let us note that the preceding construction relies on the $|\Uparrow\rangle$ state and the fact that it is an eigenstate of the B_m's, etc. However, one could also have started with a state $|\Rightarrow\rangle$ where all spins point in the x direction, which is an eigenstate of the A_e's, and then follow a similar route.

3. Construction of excited states

We now have to see how to construct excited states, i.e., states containing vortices (e or m) but still no quasiparticle. Constructing a state with some B_m's being minus one ("magnetic vortices") is easy once one has noticed that s_i^x anticommutes with two B_m's and thus changes their values to their opposite. Since s_i^x commutes with all A_e's, as well as with $\mathcal{L}^x$ and $\mathcal{L}^y$ when $\boldsymbol{i}$ does not belong to the corresponding contours, $s_i^x|\{w_p=1\},l^x,l^y\rangle_0$ is an eigenstate of the effective Hamiltonian, with two vortices living on the plaquettes touching the bond to which $\boldsymbol{i}$ belongs. (Note that since s_i^x also anticommutes with $\mathcal{L}^x$ and $\mathcal{L}^y$ when $\boldsymbol{i}$ belongs to the corresponding contours, one should use a string of s_j^x going around the torus without crossing $\mathcal{L}^x$ and $\mathcal{L}^y$ instead of s_i^x.) The corresponding state is again an equal-weight (in absolute value) superposition of states, but now with all possible open strings joining the created vortices, as well as all possible closed loops. This is illustrated in Fig. 12.

Creating "electric" vortices is easy since one can replace $\Pi_e(\frac{\mathbb{I}+A_e}{2})$ in Eq. (25) by $\Pi_e(\frac{\mathbb{I}+a_eA_e}{2})$, with $a_e=\pm1$, respecting the constraint $\Pi_e a_e=1$ [see Eq. (19)]. Such a change can also be obtained via the action of s_i^z operators. Indeed, each s_i^z operator anticommutes with two A_e's and thus changes their values to their opposite. The fluctuation of the strings induced by s_i^z operators is however hard to see with the construction we have given, which relies on the reference state $|\Uparrow\rangle$. To see this, one should construct states from the reference state $|\Rightarrow\rangle$ where all spins point in the x direction and

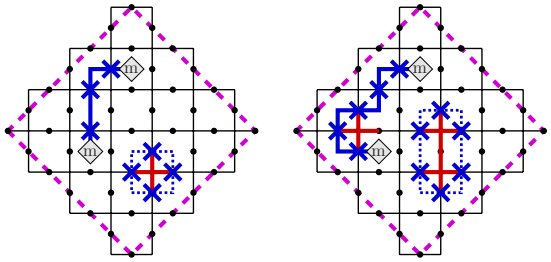

FIG. 12. (Color online) Two of the states entering the equal-weight (in absolute value) superposition for the state having two magnetic vortices. The latter are represented with little gray squares marked with the letter m and are linked with a string of spin flips [blue (dark gray) thick line]. The other graphical conventions are the same as in Fig. 9.

then use projectors involving B_m's instead of A_e's. This is not useful for our purpose so we let the interested reader doing it on his own.

4. Statistics of vortices

For completeness, let us now show that "magnetic" and "electric" vortices behave as semions with respect to each other. This is done by first creating a pair of magnetic vortices, then a pair of electric vortices, and finally by moving one of the magnetic vortices around one of the electric vortices as shown in Fig. 13 (one could also do the contrary, but then one should work with the reference state $|\Rightarrow\rangle$ to see things more easily). With the notations of this figure (see also its caption), let us consider the state $|\psi\rangle = ZX|\{w_p=1\}, l^x, l^y\rangle_0$ with two e and m vortices. Then the repeated application of spin flips along the loop X' (in any direction) moves the downmost m vortex around the leftmost e vortex. The resulting state is $X'|\psi\rangle$. But as Z and X' have one (and only one) common site, they anticommute, whereas X and X' commute so that $X'|\psi\rangle = -ZXX'|\{w_p=1\}, l^x, l^y\rangle_0$. Now, X' which is a product of s_i^x operators forming a closed loop is nothing but a product of A_e's operators (the ones enclosed in the loop). As $|\{w_p=1\}, l^x, l^y\rangle_0$ is an eigenstate of the A_e's with eigenvalue one, we finally obtain that $X'|\psi\rangle = -|\psi\rangle$: braiding a magnetic vortex around an electric vortex yields a nontrivial phase of π $(-1=e^{i\pi})$, which proves the semionic statistics.

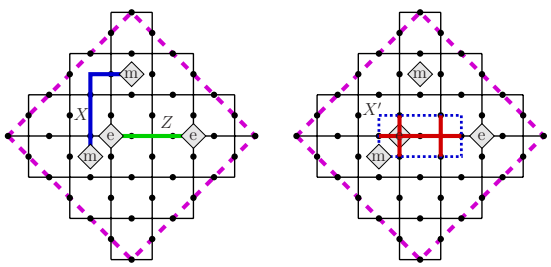

FIG. 13. (Color online) Illustration of operators involved in the braiding of a magnetic vortex around an electric vortex. X is the product $\Pi_i s_i^x$ for $\boldsymbol{i}$ belonging to the blue (dark gray) thick path linking the two m vortices (orthogonal to bonds). Z is the product $\Pi_i s_i^z$ for $\boldsymbol{i}$ belonging to the green (light gray) thick path linking the two e vortices (drawn on the bonds). X' is the product $\Pi_i s_i^x$ for $\boldsymbol{i}$ belonging to the dashed loop around the leftmost e vortex and is also equal to a product of the A_e operators encircled by the loop (denoted as thick crosses).

Let us mention that the magnetic vortices behave as bosons among themselves and so do the electric vortices. This is easily seen by noticing that creating and moving m vortices, for example, only requires s^x operators, which all commute with one another. To end this discussion about the statistics of vortices, let us also remark that a compound object made of an electric and a magnetic vortex is a fermion (see Ref. 5).

VI. EFFECTIVE HAMILTONIAN IN THE 1-QP SUBSPACE

A. Form of the Hamiltonian

The spectrum we obtained in the 0-QP subspace gives the lowest eigenenergies for each configuration of the W_p's. In this section, we explain how to compute the high-energy spectrum for states with one quasiparticle, for each W_p's configuration, and how to build the associated eigenstates. This is achieved by diagonalizing H_{eff} in the 1-QP subspace [whose dimension is $d_1 = N2^N$ (see the end of Sec. IV)]. In this subspace, the effective Hamiltonian (18) reads

$$H_{\text{eff}}|_{q=1} = E_0 + \mu - \sum_{\{p_1,\ldots,p_n\}} C_{p_1,\ldots,p_n} W_{p_1} \cdots W_{p_n} - \sum_{\{j_1,\ldots \boldsymbol{j}_n\}} D_{j_1,\ldots \boldsymbol{j}_n} S_{j_1,\ldots \boldsymbol{j}_n} b_{\boldsymbol{j}_n}^\dagger b_{j_1}, \tag{26}$$

where the second sum is performed over all non-self-retracing paths of length n starting at site $\boldsymbol{j}_1$ and ending at site $\boldsymbol{j}_n$, with possibly $\boldsymbol{j}_n = \boldsymbol{j}_1$ when working at order 4 or higher. This is the reason why we give the expansion up to this order but we would like to emphasize that obtaining orders up to 10 for $H_{\text{eff}}|_{q=1}$ is of the same complexity as for $H_{\text{eff}}|_{q=0}$. Self-retracing paths are renormalizing the chemical potential μ. Note that a hopping process of one quasiparticle around a loop is nothing but the product of the W_p's enclosed in the loop, as can be easily checked. This explains why at order 4, one obtains some terms proportional to $b_{\boldsymbol{i}}^\dagger b_{\boldsymbol{i}} W_p$, where the plaquette p shares site $\boldsymbol{i}$ (see Appendix D).

From now on $(q \geq 1)$ the phase factors appearing in the W_p's [see Eq. (14)] must be taken into account. The operators S have a structure similar to that of the W_p's, except that they are open string operators. They involve τ_j^α as well as phase factors $(-1)^{b_j^\dagger b_j}$ as follows:

$$S_{j_1,\ldots \boldsymbol{j}_n} = \varphi_{j_1,\ldots \boldsymbol{j}_n} \mathcal{T}_{j_{n-1}}^{\boldsymbol{j}_n} \cdots \mathcal{T}_{j_1}^{\boldsymbol{j}_2}, \tag{27}$$

where the $\varphi_{j_1,\ldots \boldsymbol{j}_n}$ are phase factors which reduce to the identity in the 1-QP subspace and will be discussed later on (see Sec. VII). The two-site $\mathcal{T}_{\boldsymbol{i}}^{\boldsymbol{j}}$ operators are built from the same τ_j^α operators as the hoppings $t_{\boldsymbol{i}}^{\boldsymbol{j}}$, namely,

$$\mathcal{T}_{\boldsymbol{i}}^{\boldsymbol{i}+\boldsymbol{n}_1} = \tau_{\boldsymbol{i}+\boldsymbol{n}_1}^x = (\mathcal{T}_{\boldsymbol{i}+\boldsymbol{n}_1}^{\boldsymbol{i}})^\dagger, \tag{28}$$

$$\mathcal{T}_{\boldsymbol{i}}^{\boldsymbol{i}+\boldsymbol{n}_2} = -i\tau_{\boldsymbol{i}+\boldsymbol{n}_2}^y \tau_{\boldsymbol{i}}^z = (\mathcal{T}_{\boldsymbol{i}+\boldsymbol{n}_2}^{\boldsymbol{i}})^\dagger. \tag{29}$$

Note that in the 1-QP subspace, one can also write the hopping term of the Hamiltonian as[13]

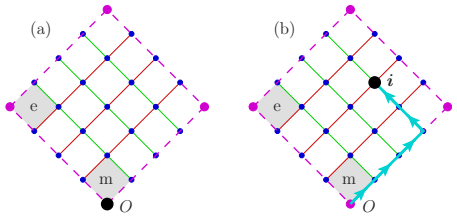

FIG. 14. (Color online) Illustration of states of the 1-QP basis, built from the ground state. (a) The action of $b_O^\dagger$ is to create a particle at site O (large black filled circle) as well as to create a pair of e and m vortices. The action of the string operator S represented with an oriented thick (cyan) line (a) on the state, then yields the state with the same vortices (b) but a particle at site $\boldsymbol{i}$. We do not bicolor the lattice in cyan (gray) and white anymore so that the figures are easier to read.

$$S_{j_1,\ldots,j_n} b_{j_n}^\dagger b_{j_1}|_{q=1} = t_{j_{n-1}}^{j_n} \cdots t_{j_1}^{j_2}. \tag{30}$$

B. Construction of a 1-QP basis

As can be seen when looking at the form of the hopping operators, bosonic and spin degrees of freedom are coupled so that one has to tackle a polaronlike problem. However, we shall now show that since all hopping operators $t_{\boldsymbol{i}}^{\boldsymbol{j}}$ commute with all W_p's as well as with all loop operators $\mathcal{L}$, the 1-QP problem is equivalent to that of one-particle hopping in a static magnetic field.

As a first step, we build a basis of the 1-QP subspace. We denote by $|\{w_p\},l^x,l^y\rangle_0$ a state of the 0-QP subspace, which is an eigenstate of the W_p's and of $\mathcal{L}^x$ and $\mathcal{L}^y$, and built as explained in Sec. V B. We choose as the origin O the site we have already denoted with a large (magenta) filled circle [see Figs. 2 and 6, as well as Fig. 14(b)]. Let us then consider the state $|\{w_p'\},l^x,l^y;O\rangle_1 = b_O^\dagger|\{w_p\},l^x,l^y\rangle_0$ belonging to the 1-QP subspace and with 1-QP at the origin. From formula (14), it is clear that adding a particle at the origin changes the value of two plaquettes, as illustrated in Fig. 14(a) for the action of $b_O^\dagger$ on the ground state, which is the reason why we made a distinction between w_p and w_p'. Note that all this is perfectly consistent with Eq. (19), as well as with the conclusion of Ref. 42. Indeed, in this paper, Levin and Wen[42] showed that fermions are always created in pairs, and this is the case here since a bound object of an electric vortex and a magnetic vortex is a fermion (see Sec. V B), and our quasiparticles will turn out to be fermions (see Sec. VII).

Other states $|\{w_p'\},l^x,l^y;\boldsymbol{i}\rangle_1$ with a particle at site $\boldsymbol{i}$ are obtained by applying an operator $S_{O,\ldots,\boldsymbol{i}} b_{\boldsymbol{i}}^\dagger b_O$ onto $|\{w_p'\},l^x,l^y;O\rangle_1$ in order to make the particle hop, without affecting the conserved $\mathbb{Z}_2$ quantities. Note that

$$S_{O,\ldots,\boldsymbol{i}} b_{\boldsymbol{i}}^\dagger b_O|\{w_p'\},l^x,l^y;O\rangle_1 = S_{O,\ldots,\boldsymbol{i}} b_{\boldsymbol{i}}^\dagger|\{w_p\},l^x,l^y\rangle_0. \tag{31}$$

However, we still need a convention for the path to be taken (which will amount to choose a gauge for the magnetic field the particles are hopping in) to obtain a well-defined basis. The path from O to $\boldsymbol{i}$ is taken to be first in the $\boldsymbol{n}_1$ direction as much as needed, then in the $\boldsymbol{n}_2$ direction. For example, in Fig. 14(b), $\boldsymbol{i}=3\boldsymbol{n}_1+2\boldsymbol{n}_2$ and the S operator is depicted as oriented thick (cyan) line in this figure, with first three move in direction $\boldsymbol{n}_1$ and then two move in direction $\boldsymbol{n}_2$.

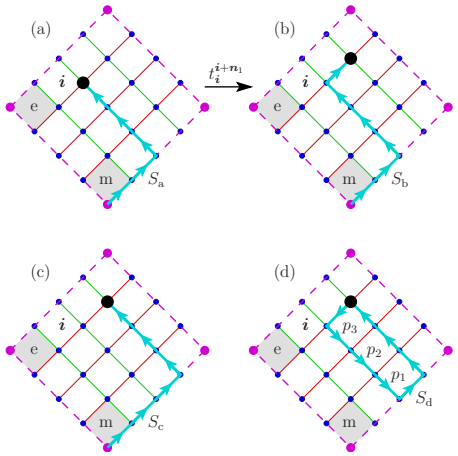

FIG. 15. (Color online) [(a)–(c)] States and (d) contour needed to compute the matrix element [Eq. (32)] (see text).

C. Hamiltonian in the 1-QP basis

Let us now consider the effective Hamiltonian at order 1, for which the hopping part is nothing but T_0, and study its action on a state $|\{w_p\},l^x,l^y;\boldsymbol{i}\rangle_1$. From the way the states have been built, it is obvious that $t_{\boldsymbol{i}}^{\boldsymbol{i}+\boldsymbol{n}_2}|\{w_p\},l^x,l^y;\boldsymbol{i}\rangle_1 = |\{w_p\},l^x,l^y;\boldsymbol{i}+\boldsymbol{n}_2\rangle_1$, and for the same reason and the fact that $\mathcal{T}_{\boldsymbol{i}}^{\boldsymbol{j}}$ is unitary, $t_{\boldsymbol{i}}^{\boldsymbol{i}-\boldsymbol{n}_2}|\{w_p\},l^x,l^y;\boldsymbol{i}\rangle_1 = |\{w_p\},l^x,l^y;\boldsymbol{i}-\boldsymbol{n}_2\rangle_1$. We then turn to the hopping term $t_{\boldsymbol{i}}^{\boldsymbol{i}+\boldsymbol{n}_1}$ and study its action on the state $|\{w_p\},l^x,l^y;\boldsymbol{i}\rangle_1$. In other words, we wish to compute the matrix element,

$$A_{\boldsymbol{i}}^{\boldsymbol{i}+\boldsymbol{n}_1} = {}_1\langle\{w_p\},l^x,l^y;\boldsymbol{i}+\boldsymbol{n}_1|t_{\boldsymbol{i}}^{\boldsymbol{i}+\boldsymbol{n}_1}|\{w_p\},l^x,l^y;\boldsymbol{i}\rangle_1. \tag{32}$$

All needed states are represented in Fig. 15: $|\{w_p\},l^x,l^y;\boldsymbol{i}\rangle_1$ in (a), $t_{\boldsymbol{i}}^{\boldsymbol{i}+\boldsymbol{n}_1}|\{w_p\},l^x,l^y;\boldsymbol{i}\rangle_1$ in (b), and $|\{w_p\},l^x,l^y;\boldsymbol{i}+\boldsymbol{n}_1\rangle_1$ in (c). Using the notations of Fig. 15 [S_a is the oriented product of spin operators $\mathcal{T}_{\boldsymbol{i}}^{\boldsymbol{j}}$ on the contour shown in (a), starting at the origin, the same for S_b and S_c, but for S_d the product starts and ends at the particle's position], it is easy to see that $S_d t_{\boldsymbol{i}}^{\boldsymbol{i}+\boldsymbol{n}_1}|\{w_p\},l^x,l^y;\boldsymbol{i}\rangle_1 = |\{w_p\},l^x,l^y;\boldsymbol{i}+\boldsymbol{n}_1\rangle_1$. Then, using the fact that $S_d^2=\mathbb{I}$,

$$A_{\boldsymbol{i}}^{\boldsymbol{i}+\boldsymbol{n}_1} = {}_1\langle\{w_p\},l^x,l^y;\boldsymbol{i}+\boldsymbol{n}_1|\, S_d\,|\{w_p\},l^x,l^y;\boldsymbol{i}+\boldsymbol{n}_1\rangle_1. \tag{33}$$

Furthermore a calculation on Pauli matrices shows that the action of S_d on the state $|\{w_p\},l^x,l^y;\boldsymbol{i}+\boldsymbol{n}_1\rangle_1$ is the same as the product of the plaquette operators encircled by the closed contour of S_d, which on the example of Fig. 15 reads $W_{p_1}W_{p_2}W_{p_3}$. We finally obtain

$$A_{\boldsymbol{i}}^{\boldsymbol{i}+\boldsymbol{n}_1} = \prod_{p\subset\mathcal{E}_{\boldsymbol{i},\boldsymbol{i}+\boldsymbol{n}_1}} w_p, \tag{34}$$

where the product has to be taken over all encircled plaquettes $\mathcal{E}_{\boldsymbol{i},\boldsymbol{i}+\boldsymbol{n}_1}$ as illustrated on a particular example in Fig. 15. The case of a hopping in the $-\boldsymbol{n}_1$ direction can of course be deduced from the above matrix elements by Hermitian conjugation.

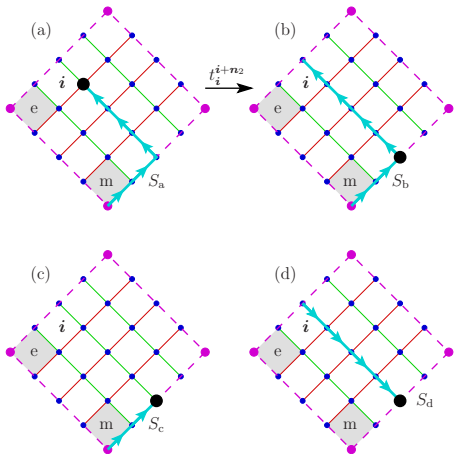

FIG. 16. (Color online) [(a)–(c)] States and (d) contour needed to compute the matrix element of a hopping in the $\boldsymbol{n}_2$ direction when site $\boldsymbol{i}$ is "one site away from the edge" of the dashed (magenta) square and (d) thus involving a loop operator (see text for details).

For some hopping processes, the matrix element not only involves a product of w_p's but also a loop operator around the torus. This is illustrated in Fig. 16 for a hopping in the $\boldsymbol{n}_2$ direction, starting from site $\boldsymbol{i}=i_x\boldsymbol{n}_1+(2p-1)\boldsymbol{n}_2$ ($i_x=2$ and $p=2$ in the figure). In this case, one has $S_d=\mathcal{L}^y_{i_x}$ (i.e., the loop operator in the y direction, around the torus, going through the sites $\boldsymbol{i}=i_x\boldsymbol{n}_1+p\boldsymbol{n}_2$, where p takes all possible values) so that

$$A_{\boldsymbol{i}}^{\boldsymbol{i}+\boldsymbol{n}_2}={}_1\langle\{w_p\},l^x,l^y;\boldsymbol{i}|t_{\boldsymbol{i}}^{\boldsymbol{i}+\boldsymbol{n}_2}|\{w_p\},l^x,l^y;\boldsymbol{i}\rangle_1=l^y_{i_x}. \tag{35}$$

As explained in Secs. II and III the value of $l^y_{i_x}$ is determined from the one of $l^y=l^y_1$ and from the value of the plaquettes in between these two loop operators.

All the above examples lead to the following conclusion. The matrix elements of the effective Hamiltonian at lowest order, in the 1-QP subspace, are the same as what one would obtain for a particle with hopping amplitudes $-J_x$ and $-J_y$ in the $\boldsymbol{n}_1$ and $\boldsymbol{n}_2$ directions of the square lattice in a magnetic field whose (reduced) fluxes in plaquettes or cycles around the torus are $\Phi/\Phi_0=0$ or $\Phi/\Phi_0=1/2$ (where Φ_0 is the flux quantum). This comes from the fact that, for example, hopping around a plaquette p gives a phase factor 1 for the two hoppings in the $\pm\boldsymbol{n}_2$ directions and an overall w_p for the hoppings in the $\pm\boldsymbol{n}_1$ directions. The overall contribution is then w_p, which takes value $w_p=\exp[2i\pi\Phi/\Phi_0]$. This analysis can be extended to the case of hoppings of the kind represented in Fig. 16 where the PBCs play a role.

When tackling higher-order corrections, hoppings become longer ranged as seen in Eq. (26), but the above considerations still apply because of Eq. (30). It is then easy to compute the 1-QP spectrum for a given map of the $\mathbb{Z}_2$ conserved quantities. As already explained, when the map does not possess translational invariance, one can only compute the spectrum numerically. When the w_p's are translationally invariant, an analytic solution is available, and for example, in the vortex-free subspace, the dispersion relation obtained at order 2 (see Appendix D) is

$$E^{\text{free}}(k_x,k_y)=1-2[J_x\cos(k_x)+J_y\cos(k_y)]+2[J_x\sin(k_x)+J_y\sin(k_y)]^2, \tag{36}$$

where the wave vector (k_x,k_y) belongs to $[-\pi,\pi]\times[-\pi,\pi]$. The gap in this sector is then obtained by minimizing E_{free}, which yields $\Delta^{\text{free}}=1-2(J_x+J_y)$. Note that, in this case, the perturbative result at order 1 coincides with the nonperturbative result obtained by Kitaev[7] (see also Sec. VIII) and one recovers the transition point at $J_x+J_y=1/2=J_z$.

Results for other sectors (vortex full or one vortex every two plaquettes) can also be obtained. We mainly used them to check the validity of the coefficients we computed perturbatively, as explained in Sec. VIII.

As a final remark about the 1-QP subspace, let us mention a difference with what is obtained when using exact fermionization methods. With these methods, the low-energy subspace already contains many fermions, and one then considers fermionic excitations on top of this complicated vacuum to reach high-energy states. In our approach, the low-energy states are really empty of fermions and the excitations are only made of one particle, which can thus be qualified of Landau quasiparticle.

VII. EFFECTIVE HAMILTONIAN IN THE ($q\geq 2$)-QP SUBSPACE

Let us now turn to multiparticle states with the aim of showing how the Fermi statistics can be recovered from hard-core bosons with a string of spin and phase operators. We shall not give many details here since our approach becomes cumbersome when studying multiparticle states and because one knows from exact solutions that one has to recover free fermions.

A. Phase factors

To obtain Fermi statistics, the phase factors appearing in the string operators S [see Eq. (18)] are of utmost importance. These factors do neither appear at the end sites of the string operators S [so in particular not at all for nearest-neighbor hoppings, which are simply the $t_{\boldsymbol{i}}^j$ operators of Eq. (13)] nor at points of turning back but only at intermediate sites between two truly different other sites. The six possibilities are shown in Fig. 17, where the phase factors occur only for the three topmost hoppings [phase factors for hoppings not represented in the figure can be inferred from Hermitian conjugation and Eq. (28)]. In the figure, oriented thick (cyan) lines represent the string operators S, and the sites $\boldsymbol{j}_2$ marked with a large dot are the ones involving a phase factor $(-1)^{b^\dagger_{j_2}b_{j_2}}$. As an example, the string operator associated to a three-site hopping as the one shown top left in Fig. 17 reads

$$S_{\boldsymbol{j},\boldsymbol{j}+\boldsymbol{n}_1,\boldsymbol{j}+2\boldsymbol{n}_1}=(-1)^{b^\dagger_{\boldsymbol{j}+\boldsymbol{n}_1}b_{\boldsymbol{j}+\boldsymbol{n}_1}}\mathcal{T}^{\boldsymbol{j}+2\boldsymbol{n}_1}_{\boldsymbol{j}+\boldsymbol{n}_1}\mathcal{T}^{\boldsymbol{j}+\boldsymbol{n}_1}_{\boldsymbol{j}}. \tag{37}$$

In fact, in $S_{\ldots,\boldsymbol{j}_1,\boldsymbol{j}_2,\boldsymbol{j}_3,\ldots}$, a phase factor appears at the intermediate site $\boldsymbol{j}_2$ if $\mathcal{T}^{\boldsymbol{j}_2}_{\boldsymbol{j}_1}$ and $\mathcal{T}^{\boldsymbol{j}_3}_{\boldsymbol{j}_2}$ commute and does not appear if they anticommute.

B. Fermionic creation operators

Rigorously, it is impossible to introduce creation or annihilation operators for single fermions because fermions

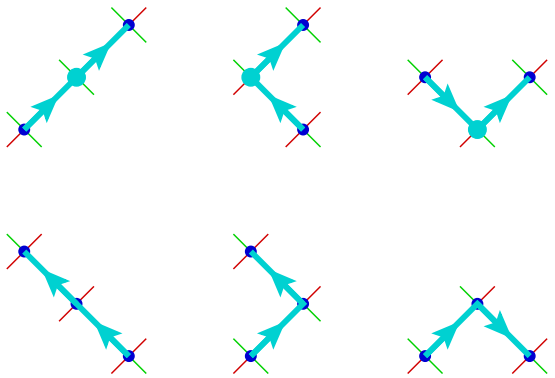

FIG. 17. (Color online) Illustration of the phase factors appearing at site $\boldsymbol{j}_2$ in the string operators $S_{\ldots,\boldsymbol{j}_1\boldsymbol{j}_2\boldsymbol{j}_3,\ldots}$. The phase factors $(-1)^{b^\dagger_{\boldsymbol{j}_2} b_{\boldsymbol{j}_2}}$ are denoted as large (cyan) dots and are only involved in the three top processes, which are, from left to right, $S_{\ldots,\boldsymbol{j}\boldsymbol{j}+\boldsymbol{n}_1\boldsymbol{j}+2\boldsymbol{n}_1,\ldots}$, $S_{\ldots,\boldsymbol{j}\boldsymbol{j}+\boldsymbol{n}_2\boldsymbol{j}+\boldsymbol{n}_1+\boldsymbol{n}_2,\ldots}$, and $S_{\ldots,\boldsymbol{j}\boldsymbol{j}-\boldsymbol{n}_2\boldsymbol{j}+\boldsymbol{n}_1-\boldsymbol{n}_2,\ldots}$.

should always be created or annihilated in pairs. In fact, after choosing a site O as an origin and after choosing a reference path from site O to site $\boldsymbol{i}$ (as was done in Sec. VI), the operator (running on this reference path) $c^\dagger_{\boldsymbol{i}} \sim S^{\mathrm{ref}}_{O,\ldots,\boldsymbol{i}} b^\dagger_{\boldsymbol{i}}$ can be considered as a fermionic creation operator at site $\boldsymbol{i}$ once the origin O has been sent to infinity (using the same trick as when constructing a Dirac monopole in electrodynamics). It should be clear from arguments similar to those of Sec. VI that such an operator creates a high-energy (spinless) fermion at site $\boldsymbol{i}$ but also creates (or destroys if there is already one) one low-energy fermion made of two vortices, top and right of site O, as in Fig. 14. It however commutes with all other W_p operators, except with these two. The fermionic anticommutation relations between fermion operators at sites $\boldsymbol{i}$ and $\boldsymbol{j}$ can be checked by exhausting all possible crossings of two reference paths $O,\ldots,\boldsymbol{i}$ and $O,\ldots,\boldsymbol{j}$.

C. Multiparticle basis and effective Hamiltonian

From there on, one can construct a multiparticle basis of the Fock space, as was done for the one-particle basis, by successively creating fermions at some sites (after having decided for an ordering of these sites). It can then be shown, as was done in the 1-QP subspace, that the Hamiltonian is nothing but a hopping Hamiltonian of free fermions in a magnetic field, whose flux per plaquette is zero or half the flux quantum ($w_p = \pm 1$). The phase factors, apart from ensuring proper Fermi statistics, also yield the correct expressions for the W_p's or product of W_p's, which involve both τ's and phase factors and which appear for hoppings around closed paths.

D. Alternative picture

As was suggested by Levin and Wen in Ref. 42, the statistics of the effective quasiparticles can be probed with a simple argument. It relies on exchanging two of these quasiparticles by using hoppings from the Hamiltonian only and doing so in such a way that a hopping on a bond between two sites as occurred exactly once in each direction in order

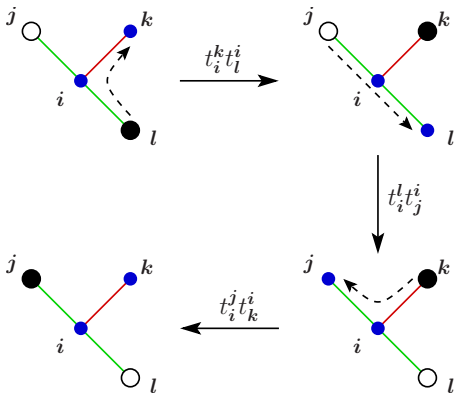

FIG. 18. (Color online) Illustration of the exchange of two particles discussed in the text for $\boldsymbol{j}=\boldsymbol{i}+\boldsymbol{n}_2$, $\boldsymbol{k}=\boldsymbol{i}+\boldsymbol{n}_1$, and $\boldsymbol{l}=\boldsymbol{i}-\boldsymbol{n}_2$.

to capture phases coming from the statistics only (and not, e.g., from a magnetic Aharonov-Bohm-type phase).

Let us, thus, consider the exchange process of two particles initially sitting at sites $\boldsymbol{j}$ and $\boldsymbol{l}$ (no other particle is present), as depicted in Fig. 18 and whose corresponding operator sequence is (using only hopping operators arising at lowest order)

$$t^j_i t^i_k t^l_i t^i_j t^k_i t^i_l = -1, \tag{38}$$

or, equivalently, $t^i_j t^k_i t^i_l = -t^i_l t^k_i t^i_j$. The sign in the latter identity confirms that the quasiparticles made of a hard-core boson and an effective spin-1/2 obey fermionic statistics.

VIII. SIMPLE CHECKS FROM SIMPLE VORTEX CONFIGURATIONS

As shown by Kitaev,[7] the spectrum of Hamiltonian (1) can be computed exactly by mapping the spin system onto free Majorana fermions. The main drawback of this mapping is that one has, first, to work in a fixed vortex sector and, in a second step, perform the symmetrization procedure involving all equivalent gauge sectors. An alternative route[9,11,12] consists in using the Jordan-Wigner transformation, which maps the problem onto free spinless fermions with p-wave pairing. However, in both approaches and as is often the case, only periodic configurations allow one to obtain analytical expressions of the spectrum. In the following, we use Kitaev's approach[6,7] (Majorana fermions) to compute the spectrum in several simple periodic configurations characterized by a filling factor $\nu = \frac{\text{No. of vortex}}{\text{No. of plaquette}}$.

Actually, diagonalizing the Majorana fermion Hamiltonian on this honeycomb lattice[7] is completely equivalent to analyzing the problem of a free particle on this lattice in a transverse magnetic field[43] with a flux per plaquette which can take only two values corresponding to $w_p = \pm 1$ (see Appendix F for details). The ground-state energy is then obtained by filling all levels with negative energy, which amounts in a bipartite lattice for which the spectrum is symmetric, to consider half filling.

For the three cases considered here, we compute the exact spectrum (still assuming $J_z \geq J_x$, $J_y \geq 0$). Then, we perform the perturbative expansion of the ground-state energy up to

order 10. This provides some simple checks of the results given in Sec. V.

A. Vortex-free configuration $\nu=0$

This configuration defined by $w_p=+1$ for all p's is of special interest since in the thermodynamical limit, the ground state of H lies in this sector. This is a direct consequence of Lieb's theorem[44] for flux phases. The spectrum, in this sector, is simply obtained since it is equivalent to compute the spectrum of a free particle in zero field. In the system being periodic with two sites per unit cell (see Fig. 1), the single-particle spectrum consists of two bands given by the roots of the following characteristic polynomial:

$$P^{\nu=0}(\varepsilon) = \varepsilon^2 - f(\mathbf{q})^2, \tag{39}$$

where for all $\mathbf{q}$ in the reciprocal lattice,

$$f(\mathbf{q})^2 = 4\{J_x^2 + J_y^2 + J_z^2 + 2[J_xJ_y\cos[\mathbf{q}\cdot(\mathbf{n}_1-\mathbf{n}_2)] + J_yJ_z\cos(\mathbf{q}\cdot\mathbf{n}_2) + J_xJ_z\cos(\mathbf{q}\cdot\mathbf{n}_1)]\}. \tag{40}$$

The ground-state energy per plaquette is thus given, in the thermodynamical limit, by

$$e_0^{\nu=0} = -\frac{1}{8\pi^2}\int_{-\pi}^{\pi} dq_x \int_{-\pi}^{\pi} dq_y |f(\mathbf{q})|. \tag{41}$$

As already found by Kitaev,[6,7] at the isotropic point $J_x=J_y=J_z=1$, one has $e_0^{\nu=0}\simeq -1.5746$.

The gap is given by the minimum, in modulus, of $P^{\nu=0}$'s roots, i.e., $\min_{\mathbf{q}}|f(\mathbf{q})|$. Thus, one obtains

$$\Delta^{\nu=0} = 2(J_z - J_x - J_y). \tag{42}$$

Setting $J_z=1/2$ and considering the perturbative limit $J_z \gg J_x, J_y$, one obtains the following expansion for the ground-state energy at order 10:

$$e_0^{\nu=0} = -\frac{1}{2} - J^2 - \frac{3J^4}{4} - \frac{5J^6}{2} - \frac{875J^8}{64} - \frac{3087J^{10}}{32}. \tag{43}$$

For simplicity, we have set here $J_x=J_y=J$. This result can be easily recovered by setting $w_p=+1$ for all p's in Eq. (21) and using the coefficients given in Appendix C. One can also check directly the one-particle spectrum by expanding $f(\mathbf{q})$ in the same limit and by comparing it with the one-particle spectrum in the vortex-free sector obtained in Sec. VI.

B. Vortex-full configuration $\nu=1$

The vortex-full sector is defined by $w_p=-1$ for all p's. In the "particle in a field" language, this problem corresponds to a magnetic flux per plaquette, which is half a flux quantum. With the gauge choice shown in Fig. 19, the system is periodic with four sites per unit cell. The single-particle spectrum, thus, consists of four bands given by the roots of the characteristic polynomial,

$$P^{\nu=1}(\varepsilon) = \varepsilon^4 - 8\varepsilon^2(J_x^2 + J_y^2 + J_z^2) + 16g(\mathbf{q})^2, \tag{44}$$

where for all $\mathbf{q}$ in the reciprocal lattice

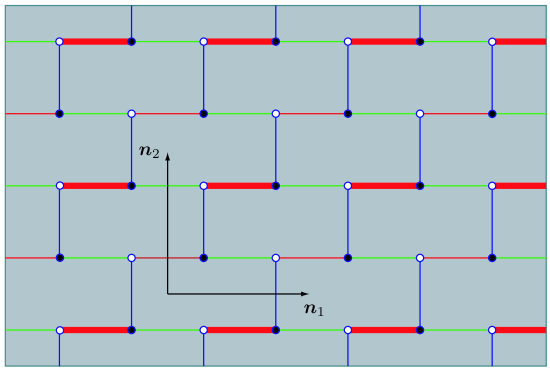

FIG. 19. (Color online) A possible gauge choice realizing the vortex-full lattice $\nu=1$. The thin (bold) links are associated to $u_{jk}=+1$ ($u_{jk}=-1$), where j belongs to the black sublattice and k to the white one (see Appendix F). The eigenvalue of the plaquette operator is then simply given by $w_p=\Pi_{(j,k)\in p}u_{jk}$.

$$g(\mathbf{q})^2 = J_x^4 + J_y^4 + J_z^4 - 2\{J_x^2J_y^2\cos(2\mathbf{q}\cdot\mathbf{n}_1) + J_y^2J_z^2\cos[\mathbf{q}\cdot(\mathbf{n}_1-\mathbf{n}_2)] - J_x^2J_z^2\cos[\mathbf{q}\cdot(\mathbf{n}_1+\mathbf{n}_2)]\}. \tag{45}$$

The vectors $\boldsymbol{n}_1=(1,0)$ and $\boldsymbol{n}_2=(0,1)$ are defined in Fig. 19. The ground-state energy per plaquette is given, in the thermodynamical limit, by

$$e_0^{\nu=1} = -\frac{\sqrt{2}}{8\pi^2}\int_{-\pi}^{\pi} dq_x \int_{-\pi}^{\pi} dq_y \sqrt{J_x^2 + J_y^2 + J_z^2 + |g(\mathbf{q})|}. \tag{46}$$

Once again, for $J_x=J_y=J_z=1$, this expression gives $e_0^{\nu=1}\simeq -1.5077$ in agreement with Kitaev's results.[7]

The gap is again given by the minimum, in modulus, of $P^{\nu=1}$'s roots

$$\Delta^{\nu=1} = 2(J_z - \sqrt{J_x^2 + J_y^2}), \tag{47}$$

in agreement with results given in Ref. 8. As for $\nu=0$, setting $J_z=1/2$ and considering the perturbative limit $J_z \gg J_x, J_y$, one obtains the following expansion for the ground-state energy at order 10:

$$e_0^{\nu=1} = -\frac{1}{2} - J^2 + \frac{J^4}{4} - \frac{3J^6}{2} + \frac{149J^8}{64} - \frac{547J^{10}}{32}. \tag{48}$$

For simplicity, we have also set here $J_x=J_y=J$. This result can be easily recovered by setting $w_p=-1$ for all p in Eq. (21) and using the coefficients given in Appendix C.

C. Vortex-half configuration $\nu=1/2$

Let us now consider the vortex-half configuration shown in Fig. 20, which is made of alternating vortex-free and vortex-full rows. With the gauge choice shown in this figure, the system is periodic with eight sites per unit cell. The eight bands of the single-particle spectrum are given from the roots of the following characteristic polynomial:

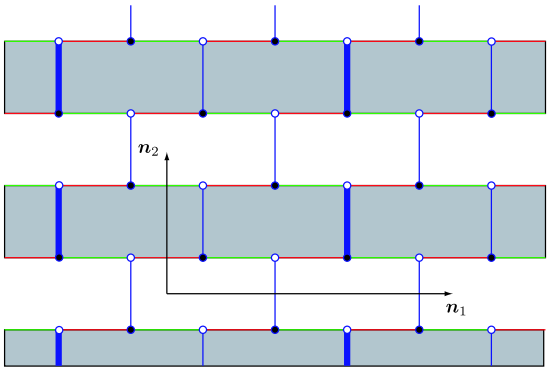

FIG. 20. (Color online) A possible gauge choice realizing the vortex-half lattice $\nu=1/2$. Notations are the same as in Fig. 19. In this configuration, vortices are localized in alternance on horizontal rows.

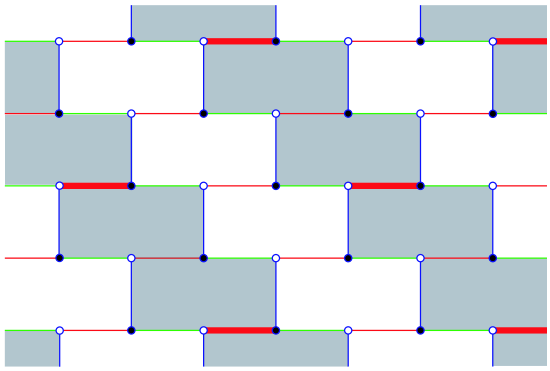

FIG. 21. (Color online) Another possible gauge choice realizing the vortex-half lattice $\nu=1/2$. Notations are the same as in Fig. 19. In this configuration, vortices are localized, in alternance, on diagonal bands.

$$
\begin{aligned}
P^{\nu=1/2}(\varepsilon) = {} & \varepsilon^8 - 16\varepsilon^6(J_x^2+J_y^2+J_z^2) + 32\varepsilon^4[3(J_x^4+J_y^4+J_z^4) \\
& + 4(J_x^2J_y^2+J_y^2J_z^2+J_x^2J_z^2) - 2J_x^2J_y^2\cos(\mathbf{q}\cdot\mathbf{n}_1)] \\
& - 256\varepsilon^2[J_x^6+J_y^6+J_z^6+(J_x^2+J_y^2)(J_y^2+J_z^2)(J_x^2+J_z^2) \\
& - 2J_x^2J_y^2(J_x^2+J_y^2)\cos(\mathbf{q}\cdot\mathbf{n}_1)] + 256\{J_x^8+J_y^8+J_z^8 \\
& + 4J_x^4J_y^4 - 4(J_x^2J_y^6+J_x^6J_y^2)\cos(\mathbf{q}\cdot\mathbf{n}_1) \\
& + 2J_x^2[J_x^2J_y^4\cos(2\mathbf{q}\cdot\mathbf{n}_1) - J_y^2J_z^4\cos(2\mathbf{q}\cdot\mathbf{n}_2)] \\
& + 2J_z^4\{J_x^4\cos[\mathbf{q}\cdot(\mathbf{n}_1+2\mathbf{n}_2)] \\
& + J_y^4\cos[\mathbf{q}\cdot(\mathbf{n}_1-2\mathbf{n}_2)]\}\}.
\end{aligned}
$$

The vectors $\boldsymbol{n}_1=(1,0)$ and $\boldsymbol{n}_2=(0,1)$ are defined in Fig. 20. Note that since the hexagonal lattice is bipartite, the single-particle spectrum is even and, consequently, all characteristic polynomials are functions of ε^2. Thus, even in this vortex-half configuration, one can get analytical expressions for the eight bands since, practically, one only has to find the roots of a fourth-order polynomial.

At the isotropic point, one obtains the ground-state energy per plaquette $e_0^{\nu=1/2}\simeq -1.5227$. The gap is given by the minimum, in modulus, of $P^{\nu=1/2}$'s roots,

$$\Delta^{\nu=1/2} = 2(J_z - \sqrt{J_x^2+J_y^2}). \tag{49}$$

It is worth noting that the gap in this sector is exactly the same as the one in the vortex-full sector $\Delta^{\nu=1}$ [see Eq. (47)].

Expanding the negative roots of $P^{\nu=1/2}$ at order 10 and integrating them out as in the previous sector, one gets for $J_x=J_y=J$,

$$e_0^{\nu=1/2} = -\frac{1}{2} - J^2 - \frac{J^4}{4} + \frac{3J^6}{2} - \frac{411J^8}{64} - \frac{211J^{10}}{32}. \tag{50}$$

Finally, one may also consider another vortex-half configuration rotated as shown in Fig. 21. The corresponding characteristic polynomial is straightforwardly obtained from $P^{\nu=1/2}$ by the permutation $J_x\to J_y$, $J_y\to J_z$, and $J_z\to J_x$. However, since the perturbation is performed in the limit $J_z \gg J_x, J_y$ it leads to a different expression for the expanded ground-state energy. In this case, one gets for $J_x=J_y=J$,

$$e_0^{\nu=1/2} = -\frac{1}{2} - J^2 - \frac{J^4}{4} - \frac{J^6}{4} + \frac{109J^8}{64} + \frac{59J^{10}}{16}. \tag{51}$$

Once again, both expressions (50) and (51) can be recovered from Eq. (21) using the coefficients given in Appendix C.

The various results obtained for $\nu=0,1,1/2$ provide (partial) checks of the coefficients given in Appendixes C and D and show the power of the PCUTs to compute high-order expansion for the spectrum. In Sec. IX, we shall show that this method is also an efficient tool to tackle more complex problems.

IX. OBSERVABLES

One of the advantages of the CUT method is that it allows one to obtain the effective form of any observables and to compute its matrix elements in the eigenbasis of the Hamiltonian. The aim of this section is twofold. First, we compute perturbatively the spin-spin correlations and show that they admit a plaquette-operator expansion similar to that of the spectrum. The second part of this section is dedicated to the most fundamental problem of local spin operations onto the ground state. Following Ref. 16, we show that single-spin operations create not only anyons but also fermions. We compute the spectral weights of various states stemming from such operations, and we also analyze the action of string operations which allow for manipulation of anyons. Finally, we give a procedure to derive the operators which create anyons without fermions and show that they involve tricky superpositions of multispin operators.

A. Spin-spin correlation functions

Hamiltonian (1) is invariant under the time-reversal symmetry since it is a quadratic function of the spin operators. Thus, any expectation value of an odd number of spin operators vanishes (such as the magnetization $\langle\sigma_i^\alpha\rangle$). Note also that the absence of odd cycles ensures that the eigenstates do not break this symmetry.[7,26,27]

In addition, the only nonvanishing spin correlators are those involving products of $\sigma_i^\alpha\sigma_j^\alpha$ on α dimers.[12,17,18] In this section, we focus on the spin-spin correlation functions and

their expression in the 0-QP sector. More precisely, we consider the following operators: $C_{i,j}^{\alpha\alpha}=\sigma_i^\alpha\sigma_j^\alpha$, where (i,j) is an α dimer. To compute these quantities, we proceed in a way similar to what we have already done to derive the effective Hamiltonian:

(i) we express the observable in the ESB language;

(ii) we compute its effective form perturbatively as explained in Appendix B (see also Ref. 45 for a detailed discussion); and

(iii) we project it out in the sector of interest.

Using the ESB form of the spin operators [Eq. (8)], we straightforwardly achieve the first step mentioned above for the three correlation functions,

$$\sigma_{i,\circ}^x\sigma_{i+\boldsymbol{n}_1,\bullet}^x=(b_i^\dagger+b_i)\tau_{i+\boldsymbol{n}_1}^x(b_{i+\boldsymbol{n}_1}^\dagger+b_{i+\boldsymbol{n}_1}), \tag{52}$$

$$\sigma_{i,\circ}^y\sigma_{i+\boldsymbol{n}_2,\bullet}^y=\mathrm{i}\tau_i^z(b_i^\dagger-b_i)\tau_{i+\boldsymbol{n}_2}^y(b_{i+\boldsymbol{n}_2}^\dagger+b_{i+\boldsymbol{n}_2}), \tag{53}$$

$$\sigma_{i,\circ}^z\sigma_{i,\bullet}^z=1-2b_i^\dagger b_i=(-1)^{b_i^\dagger b_i}. \tag{54}$$

To avoid any ambiguity, we keep track of the type of sites ($\bullet$ or $\circ$) but we are working, at this stage, on the effective square lattice. Next, we turn to the second step using the perturbative expansion described in Appendix B. In the present case, we pushed the calculation up to order 6 and, finally, we focus on the 0-QP sector.

As one expects, the effective form of the spin-spin correlation function is similar to that of the effective Hamiltonian. This is due to the fact that in the low-energy sector, W_p's are the only degrees of freedom. Thus, we obtain, an expansion in terms of the plaquette operators,

$$C_{ij}^{\alpha\alpha}|_{q=0}=a^{\alpha\alpha}-\sum_{\{p_1,\ldots,p_n\}}b_{p_1,\ldots,p_n}^{\alpha\alpha}W_{p_1}\cdots W_{p_n}. \tag{55}$$

The coefficients $a^{\alpha\alpha}$ and $b_{p_1,\ldots,p_n}^{\alpha\alpha}$ are given in Appendix E up to order 6. Here again, we can see that these correlation functions involve interactions between connected or disconnected plaquettes.

As a simple check of our expression, one can easily compute the nonperturbative correlation function in the vortex-free and the vortex-full sectors, thanks to the Hellman-Feynman theorem. Indeed, in these sectors, all sites are equivalent so that one readily gets the expectation value,

$$\langle C_{ij}^{\alpha\alpha}|_{q=0}\rangle_\nu=C_{ij}^{\alpha\alpha}|_{q=0}^\nu=-\frac{\partial e_0^\nu}{\partial J_\alpha} \tag{56}$$

for both cases $\nu=0,1$ for which the ground-state energies are given in Eqs. (41) and (46). As in Sec. VIII, the subscript ν indicates that we consider the ground state of the sector with filling factor $\nu=0,1$. Then, expanding these expressions (before derivation) and setting $J_z=1/2$ and for simplicity $J_x=J_y=J$, one gets

$$C_i^{zz}|_{q=0}^{\nu=0}=1-2J^2-\frac{9J^4}{2}-25J^6, \tag{57}$$

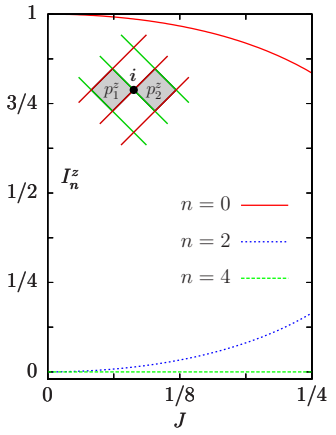

FIG. 22. (Color online) Behavior of the spectral weights I_n^z for fermion numbers $n=0,2,4$ as a function of the coupling $J=J_x=J_y$ for $J_z=1/2$. Gray plaquettes in the insets show the positions p_1^z and p_2^z at which the anyons are created under the action of τ_i^z.

$$C_{ij}^{xx}|_{q=0}^{\nu=0}=J+\frac{3J^3}{2}+\frac{15J^5}{2}=C_{ij}^{yy}|_{q=0}^{\nu=0} \tag{58}$$

for the vortex-free sector and

$$C_i^{zz}|_{q=0}^{\nu=1}=1-2J^2+\frac{3J^4}{2}-15J^6, \tag{59}$$

$$C_{ij}^{xx}|_{q=0}^{\nu=1}=J-\frac{J^3}{2}+\frac{9J^5}{2}=C_{ij}^{yy}|_{q=0}^{\nu=1} \tag{60}$$

for the vortex-full sector. As can be checked, these results can be recovered using the coefficients given in Appendix E and Eq. (55). We emphasize that, as for the spectrum, our expressions allow us to investigate arbitrary vortex configurations such as sparse vortex ones, recently studied numerically.[14,23]

B. Creation of anyons

Let us now analyze the action of a single-spin operation onto the ground state, and following Ref. 16, let us focus on $\sigma_{i,\bullet}^z$. As for the correlation functions, one first has to write this operator in the ESB formalism, which is, again, straightforward since $\sigma_{i,\bullet}^z=\tau_i^z$. Then, one computes its renormalization under the unitary transformation U which "diagonalizes" the Hamiltonian. Finally, one can compute any matrix element of this observable between any eigenstates.

At order 0, the observable is not renormalized and one has $U^\dagger\tau_i^zU=\tau_i^z$. When this operator acts onto the ground state which is in the vortex-free sector, it thus simply flips the two plaquettes as shown in Fig. 22. In other words, it creates two anyons and nothing else.

At order 1, one gets

$$U^\dagger\tau_i^zU=\tau_i^z[1+(J_xv_{i-\boldsymbol{n}_1}^i+J_yv_{i-\boldsymbol{n}_2}^i+\mathrm{H.c.})], \tag{61}$$

showing that things are more complex since pairs of particles (fermions) are created. It means that, at this order, τ_i^z couples the 0-QP subspace of the vortex-free sector with the two-

quasiparticle (2-QP) subspace of the two-vortex sector discussed above. To have a physical quantitative picture of such processes, let us compute the spectral weights defined as

$$I_n^z = \sum_{\boldsymbol{k}} |\langle \{p_1^z, p_2^z\}, n, \boldsymbol{k} | \tau_{\boldsymbol{i}}^z | 0 \rangle|^2, \tag{62}$$

where $|\{p\}, n, \boldsymbol{k}\rangle$ denotes the eigenstate of H in a sector given by an anyon configuration $w_p = -1$ and n denotes high-energy quasiparticles with quantum numbers $\boldsymbol{k}$. Here, the plaquettes p_1^z and p_2^z are as indicated in the inset of Fig. 22. This quantity measures the weight of all n-fermion contributions obtained by the action of $\tau_{\boldsymbol{i}}^z$ onto the ground state $|0\rangle$, which contains no fermions and no anyons. As it should be, these spectral weights satisfy the sum rule $\Sigma_n I_n^z = 1$. At order 6, one gets

$$I_0^z = 1 - (J_x^2 + J_y^2) - \frac{3}{2}(J_x^4 + J_y^4) - 4J_x^2 J_y^2 - \frac{7}{2}(J_x^6 + J_y^6) - \frac{43}{2}(J_x^2 J_y^4 + J_x^4 J_y^2), \tag{63}$$

$$I_2^z = J_x^2 + J_y^2 + \frac{3}{2}(J_x^4 + J_y^4) + 4J_x^2 J_y^2 + \frac{7}{2}(J_x^6 + J_y^6) + \frac{43}{2}(J_x^2 J_y^4 + J_x^4 J_y^2), \tag{64}$$

which show the importance of the two-fermion states for increasing couplings, as can be seen in Fig. 22. Note that the sum rule is fulfilled here implying $I_{n\geq 4}^z = 0$ at order 6. Actually, one may consider representative curves in Fig. 22 as almost converged since order 8 corrections would bring very small corrections. To summarize, one must realize that local spin operations onto the ground state create anyons (here two) but also give rise to fermionic excitations whose weight increases significantly with the perturbation.

C. Manipulation of anyons

Another important question concerns the manipulation of the anyons, which, as shown above, may be created by local spin operations. Such an issue is of special interest for experiments aiming at braiding anyons.[30] This topic has been the subject of a recent controversy with Zhang *et al.*[33,46] who completely neglected the existence of fermions in this model. Following Jiang *et al.*[30] who proposed an ingenious protocol to detect anyon statistics, we wish to compute the action of a string operator onto the ground state.

For simplicity, we consider here the operator $S = \Pi_{a=1,m} \sigma_{i_a,\bullet}^z$ along a horizontal line of the original brick-wall lattice (see Fig. 23 with $m=3$ for notations). At order 0, it is simple to see that S first creates two anyons and makes one of them jump in the direction of the string so that, at the end, one eventually has one anyon at plaquette 1, another anyon at the plaquette $m+1$, and no fermion.

However, at higher orders, as previously, such an operation creates fermions. To quantify this phenomenon, we consider the probability $\mathcal{P} = |\langle \{1, m+1\}, 0 | S | 0 \rangle|^2$ to find the final state in the lowest-energy state (no fermions) with anyons at

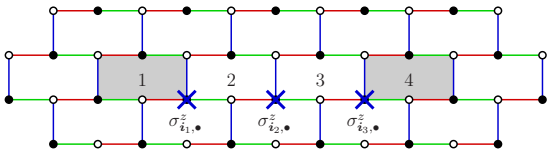

FIG. 23. (Color online) Action, in the vortex-free sector, of the string operator $S = \sigma_{i_3,\bullet}^z \sigma_{i_2,\bullet}^z \sigma_{i_1,\bullet}^z$. Each operator flips the two plaquettes adjacent to the z dimer; it is attached to but also creates fermionic excitations (not shown).

plaquettes 1 and $(m+1)$, which coincides with I_0^z for $m=1$. In Ref. 16, we computed this probability at order 2, but here we go beyond and give the result at order 6,

$$\mathcal{P} = 1 - m(J_x^2 + J_y^2) + \frac{m(m-4)}{2}(J_x^4 + J_y^4) + (m^2 - 8m + 3)J_x^2 J_y^2 - \frac{m(m^2 - 12m + 32)}{6}(J_x^6 + J_y^6) + \left(-\frac{m^3}{2} + 10m^2 - 51m + 20\right)(J_x^4 J_y^2 + J_x^2 J_y^4). \tag{65}$$

The main reason to perform this high-order calculation is that the above expression pleads in favor of an exponentiated form linear with m. Indeed, although we have no proof, we conjecture that $\mathcal{P}$ can be recast into $\exp(A - mB)$ as suggested in footnote 4 of Ref. 7. It is indeed striking to see that expression (65), which is a polynomial of the variable m, can be seen as the expansion of such a simple form with, at order 6,

$$A = 3J_x^2 J_y^2 + 20(J_x^4 J_y^2 + J_x^2 J_y^4), \tag{66}$$

$$B = J_x^2 + J_y^2 + 8J_x^2 J_y^2 + 2(J_x^4 + J_y^4) + 48(J_x^4 J_y^2 + J_x^2 J_y^4) + \frac{16}{3}(J_x^6 + J_y^6). \tag{67}$$

Further, it is clear that $\mathcal{P}$ is bounded by 0 and 1 for any m, which is clearly not the case if one considers Eq. (65). Let us also note that the fact that $U^\dagger \tau_{\boldsymbol{i}}^z U$ is found to be proportional to $\tau_{\boldsymbol{i}}^z$ [see Eq. (61)], strengthen the idea of an exponential form of this effective observable and hence for S.

We display the results at various order in Fig. 24 using expanded form (65) and the exponential form. As can be clearly seen, the exponential form seems to be well behaved. In addition, the order 6 expansion of A and B seems to provide an almost converged result when put in the exponential. Thus, we claim that one can use this form to obtain a very accurate value of $\mathcal{P}$, which is known to be of primer interest for braiding experiments.[16,30–32]

D. Anyons without fermions

As discussed previously, local or string spin operations create fermions. However, in experiments, one wishes to manipulate anyons without being spoiled by these fermions.[30] In other words, the ideal operations would consist in exciting plaquettes (only) while remaining in the ground state of the

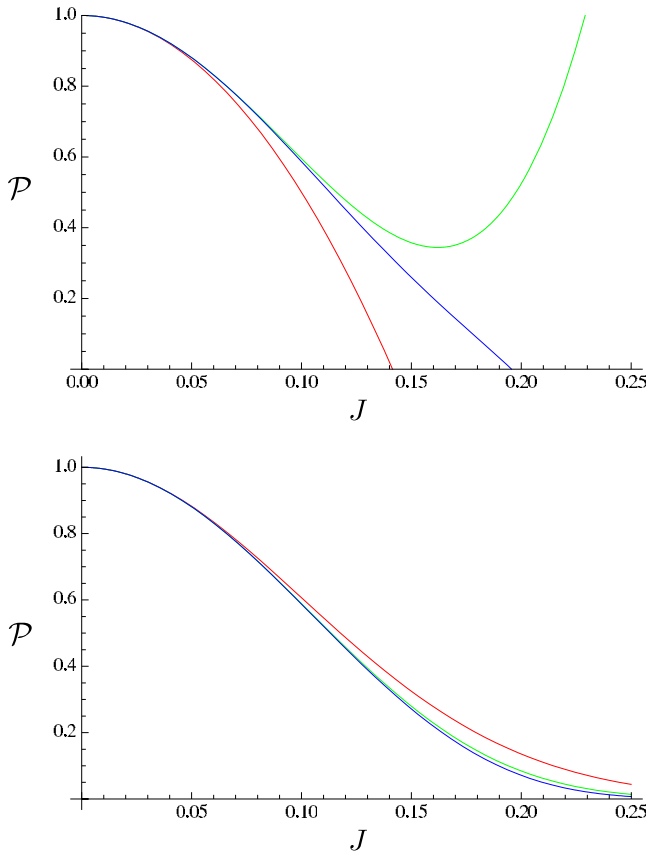

FIG. 24. (Color online) $\mathcal{P}$ as a function of $J_x=J_y=J$ computed for $m=25$. Top: nonresummed (bare) expression (65) at order 2 [red (bottom)], 4 [green (top)], and 6 [blue (middle)]. Bottom: exponentiated form $\exp(A-mB)$ at order 2 [red (top)], 4 [green (middle)], and 6 [blue (bottom)].

corresponding vortex sector. In this section, we shall show, perturbatively, that it is possible to do so even if the form of such operators is hard to implement in realistic devices.

As an example, let us determine the operator $\Omega_{\boldsymbol{i}}$ creating two vortices at the left and right plaquettes of a given site $\boldsymbol{i}$ [see inset of Fig. 22 (left)]. This operator must be such that $\Omega_{\boldsymbol{i}_{\text{eff}}}=U^\dagger\Omega_{\boldsymbol{i}}U=\tau^z_{\boldsymbol{i}}$, which indeed leads to $I^z_0=1$. Note that this procedure is the inverse of what is usually done with CUTs since, here, we wish to compute the bare observable given the effective observable instead of the opposite.

Let us assume that this operator has a perturbative expansion, namely,

$$\Omega_{\boldsymbol{i}}=\sum_{k\in\mathbb{N}}\Omega^{(k)}_{\boldsymbol{i}}, \tag{68}$$

where $\Omega^{(k)}_{\boldsymbol{i}}$ contains all operators of order k and thus associated to $J_x^l J_y^m$ (with $l+m=k$). At order 0, operators are not renormalized so that one obviously has $\Omega^{(0)}_{\boldsymbol{i}}=\tau^z_{\boldsymbol{i}}$. The renormalization of $\Omega_{\boldsymbol{i}}$ under the unitary transformation U reads

$$\Omega_{\boldsymbol{i}_{\text{eff}}}=\sum_{k\in\mathbb{N}}\Omega^{(k)}_{\boldsymbol{i}_{\text{eff}}}=\sum_{k\in\mathbb{N}}U^\dagger\Omega^{(k)}_{\boldsymbol{i}}U=\sum_{k\in\mathbb{N}}\sum_{l\in\mathbb{N}}\Omega^{(k),[l]}_{\boldsymbol{i}_{\text{eff}}}, \tag{69}$$

where $\Omega^{(k),[l]}_{\boldsymbol{i}_{\text{eff}}}$ is of order $(k+l)$. Since, at order 0, one has $\Omega_{\boldsymbol{i}_{\text{eff}}}=\tau^z_{\boldsymbol{i}}$, one must have, at each order $r>0$,

$$\sum_{k\in\mathbb{N}}\sum_{l\in\mathbb{N}}\Omega^{(k),[l]}_{\boldsymbol{i}_{\text{eff}}}=0, \tag{70}$$

where the sum is restricted to values of indices such that $k+l=r$. At order 1, this leads to

$$\Omega^{(0),[1]}_{\boldsymbol{i}_{\text{eff}}}+\Omega^{(1),[0]}_{\boldsymbol{i}_{\text{eff}}}=0. \tag{71}$$

Using Eq. (61) and the fact that $\Omega^{(k),[0]}_{\boldsymbol{i}_{\text{eff}}}=\Omega^{(k)}_{\boldsymbol{i}}$, one then obtains

$$\Omega^{(1)}_{\boldsymbol{i}}=-(J_x v^{\boldsymbol{i}}_{\boldsymbol{i}-\boldsymbol{n}_1}+J_y v^{\boldsymbol{i}}_{\boldsymbol{i}-\boldsymbol{n}_2}+\text{H.c.}). \tag{72}$$

Using the inverse mapping of Eq. (8),

$$\tau^x_{\boldsymbol{i}}=\sigma^x_{\boldsymbol{i},\bullet}\sigma^x_{\boldsymbol{i},\circ}, \tag{73}$$

$$\tau^y_{\boldsymbol{i}}=\sigma^y_{\boldsymbol{i},\bullet}\sigma^x_{\boldsymbol{i},\circ}, \tag{74}$$

$$\tau^z_{\boldsymbol{i}}=\sigma^z_{\boldsymbol{i},\bullet}, \tag{75}$$

$$b^\dagger_{\boldsymbol{i}}=\frac{1}{2}(\sigma^x_{\boldsymbol{i},\circ}-\mathrm{i}\sigma^z_{\boldsymbol{i},\bullet}\sigma^y_{\boldsymbol{i},\circ}), \tag{76}$$

one finally gets, in the original spin language and at order 1,

$$\Omega_{\boldsymbol{i}}=\Omega^{(0)}_{\boldsymbol{i}}+\Omega^{(1)}_{\boldsymbol{i}} \tag{77}$$

$$=\sigma^z_{\boldsymbol{i},\bullet}+\frac{1}{2}[J_x(\sigma^z_{\boldsymbol{i}-\boldsymbol{n}_1,\bullet}\sigma^y_{\boldsymbol{i}-\boldsymbol{n}_1,\circ}\sigma^y_{\boldsymbol{i},\bullet}-\sigma^x_{\boldsymbol{i}-\boldsymbol{n}_1,\circ}\sigma^x_{\boldsymbol{i},\bullet}\sigma^z_{\boldsymbol{i},\circ})$$
$$+J_y(\sigma^z_{\boldsymbol{i}-\boldsymbol{n}_2,\bullet}\sigma^x_{\boldsymbol{i}-\boldsymbol{n}_2,\circ}\sigma^x_{\boldsymbol{i},\bullet}-\sigma^y_{\boldsymbol{i}-\boldsymbol{n}_2,\circ}\sigma^y_{\boldsymbol{i},\bullet}\sigma^z_{\boldsymbol{i},\circ})]. \tag{78}$$

This expression shows that to create anyons without fermions, one has to build a complex superposition of operators with fine-tuned coefficients. At order 1 considered here, such states require single and triple spin-flip operations but, of course, higher-order corrections would involve higher-order spin-flip processes. Such constraints make creation of anyons without fermions via local operations difficult experimentally.[16]

X. CONCLUSION AND PERSPECTIVES

We have analyzed perturbatively the gapped phase of the Kitaev honeycomb model[6,7] in the isolated-dimer limit using the continuous unitary transformations. We have, thus, derived the low-energy effective theory up to order 10, which has been found to describe an interacting-anyon system. This result has to be contrasted with the order 4 result which predicts a free anyon system.[7] We also showed that the excitations in each vortex sector obey fermionic statistics.

In a second step, we focused on the action of local spin operators onto the ground state and we have shown that they generate both anyons and fermions. We also gave the form of the operator which creates anyons without fermions. This operator involves multispin operators which may be hard to implement experimentally.

Of course, several questions remain open in this model. As explained by Kitaev,[6,7] there exists a gapless phase which

is associated to non-Abelian anyons. The influence of a magnetic field in this phase is certainly one of the most challenging question and should reveal rich phenomena. Note that the effect of a magnetic field in the toric code already gives rise to a nontrivial phase diagram as recently discussed in Refs. 47 and 48.

Another interesting issue concerns the time evolution of local excitations. Indeed, in Sec. IX C, we discussed the effect of a string operator onto the ground state but we always considered static quantities. Although experimentally, successive spin operations may be performed on "short" time scales, it would be of primer interest to compute the spreading of fermionic excitations during the braiding processes proposed to detect anyons.[30]

ACKNOWLEDGMENTS

We wish to thank M. Kamfor for a careful reading of the manuscript. K.P.S. acknowledges ESF and EuroHorcs for funding through EURYI.

APPENDIX A: STRUCTURE OF THE EFFECTIVE HAMILTONIAN

As we have seen in Sec. III, when setting $J_z=1/2$, Hamiltonian (1) can be written as

$$H=-\frac{N}{2}+Q+T_0+T_{+2}+T_{-2}, \tag{A1}$$

where N is the number of z dimers, Q is the particle-number operator, T_0 contains the pure hopping operators which does not change the number of particles, and T_{+2} (T_{-2}) creates (annihilates) pairs of particles. The operators $T_{0,\pm 2}$ are proportional to the small parameters from which the perturbation theory is performed.

The idea of the present approach is to transform Hamiltonian (9) into an effective one which conserves the particle number. Of course, in general, this cannot be achieved exactly and, as often, one has to perform a perturbative expansion. To achieve this goal, a very powerful tool is the continuous unitary transformation method.[34] For the problem at hand, Knetter and Uhrig[39] developed a code which computes the coefficients of this expansion at high orders.[49] Practically, one must keep in mind that at order 10, which is the maximum order considered in this paper, one already has more than 10^4 terms. We refer the interested reader to Ref. 39 for a detailed derivation and we give below, for illustration, the results up to order 4.

The operators and corresponding coefficients are set in Table I, together with the lowest number $q_{\min}$ of particles such that the operator has, *a priori*, a nonzero action within the q-particle subspace for $q \geq q_{\min}$. $q_{\min}$ is found by requiring that the number of particles in the system is always positive *and* by using the fact that T_0 projects out zero-particle states. Note that some terms may vanish for more subtle reasons. For example, the third-order term $T_{-2}T_0T_{+2}$ does not act on the 0-QP states. Indeed, T_{+2} creates a 2-QP state; then T_0 makes one of the particle hops; and finally T_{-2} tries to annihilate two particles, but cannot, since these are not nearest neighbor anymore due to the hopping.

TABLE I. Operators appearing in H_{eff} with its corresponding coefficient up to order 4, together with the q-particle subspace they start to act on.

Order	Operator O	Coefficient c	$q_{\min}$
1	T_0	1	1
2	$T_{-2}T_{+2}$	$-1/2$	0
2	$T_{+2}T_{-2}$	1/2	2
3	$T_{-2}T_0T_{+2}$	1/4	0
3	$T_0T_{-2}T_{+2}$	$-1/8$	1
3	$T_{-2}T_{+2}T_0$	$-1/8$	1
3	$T_{+2}T_{-2}T_0$	$-1/8$	2
3	$T_0T_{+2}T_{-2}$	$-1/8$	2
3	$T_{+2}T_0T_{-2}$	1/4	3
4	$T_{-2}T_{-2}T_{+2}T_{+2}$	$-1/16$	0
4	$T_{-2}T_0T_0T_{+2}$	$-1/8$	0
4	$T_{-2}T_{+2}T_{-2}T_{+2}$	1/8	0
4	$T_0T_{-2}T_0T_{+2}$	1/8	1
4	$T_0T_0T_{-2}T_{+2}$	$-1/32$	1
4	$T_{-2}T_0T_{+2}T_0$	1/8	1
4	$T_0T_{-2}T_{+2}T_0$	$-1/16$	1
4	$T_{-2}T_{+2}T_0T_0$	$-1/32$	1
4	$T_{+2}T_{-2}T_0T_0$	1/32	2
4	$T_0T_{+2}T_{-2}T_0$	1/16	2
4	$T_0T_0T_{+2}T_{-2}$	1/32	2
4	$T_{+2}T_{-2}T_{+2}T_{-2}$	$-1/8$	2
4	$T_{+2}T_0T_{-2}T_0$	$-1/8$	3
4	$T_0T_{+2}T_0T_{-2}$	$-1/8$	3
4	$T_{+2}T_0T_0T_{-2}$	1/8	3
4	$T_{+2}T_{+2}T_{-2}T_{-2}$	1/16	4

One can then directly write the effective Hamiltonian,

$$H_{\text{eff}}=-\frac{N}{2}+Q+\sum_i c_i O_i, \tag{A2}$$

where O_i is the ith element of the column "operator" of Table I and c_i is the associated coefficient, the order being given by the first column. By construction, the effective Hamiltonian conserves the particle number and the energy states are ordered according to their quasiparticle number, the ground state being in the 0-QP sector. Furthermore, since $[H_{\text{eff}},Q]=0$, one may also rewrite the effective Hamiltonian in the following form:

$$H_{\text{eff}}=\sum_{q\in\mathbb{N}} H_{\text{eff}}|_q, \tag{A3}$$

where $H_{\text{eff}}|_q$ denotes the projection of H_{eff} onto the q-QP sector. Note that it is not the decoupling used in the CUT community where usually one gathers all operators which contain exactly q creation and q annihilation operators and, thus, act on the q'-QP sector with $q' \geq q$.

Finally, one must analyze each sector defined by the number of quasiparticles and determine the action of each operator O_i in the corresponding subspace. This is the nontrivial part of the job which depends on the problem under consideration. Let us emphasize that if each operator only starts to act in the $q_{\min}$-QP sector, it has also, in general, a nontrivial action on the q-QP sectors for $q > q_{\min}$.

APPENDIX B: PERTURBATIVE EXPANSION OF OBSERVABLES

In this appendix, we give the general perturbative expansion of any observable Ω obtained with the CUTs using the quasiparticle number-conserving generator. As is the case for the Kitaev model,[6,7] we suppose that the Hamiltonian of the system can be cast in the following form:

$$H = Q + T_{-2} + T_0 + T_{+2}, \tag{B1}$$

and it satisfies the hypothesis given after Eq. (16). In this case, the flow equations obtained from the CUT method can be solved perturbatively,[45] and the effective observable can be written as

$$\Omega_{\text{eff}} = \Omega + \sum_i c_i O_i, \tag{B2}$$

where O_i is the ith element of the column operator of Table II and c_i is the associated coefficient, the order being given by the first column.

At order 6 considered in this paper for the correlation functions, there are several thousands of terms to consider. Once this effective form is derived, one then has to analyze it in the quasiparticle sector of interest as done for the effective Hamiltonian.

APPENDIX C: COEFFICIENTS OF THE PERTURBATIVE EXPANSION OF THE HAMILTONIAN IN THE 0-QP SECTOR

As explained in Sec. V, the effective Hamiltonian in the 0-QP sector schematically reads

$$H_{\text{eff}}|_{q=0} = E_0 - \sum_{\{p_1,\ldots,p_n\}} C_{p_1,\ldots,p_n} W_{p_1} \cdots W_{p_n}, \tag{C1}$$

where $\{p_1,\ldots,p_n\}$ denotes a set of n plaquettes and W_p are conserved plaquette operators. The form of the effective Hamiltonian is translationally invariant (of course the configuration of the w_p's need not be) so that $C_{p_1,\ldots,p_n}$, in fact, only depends on relative coordinates of the plaquettes, and we will use (except for the one-plaquette coefficient) the notation $\tilde{C}_{p_2-p_1,\ldots,p_n-p_1} = C_{p_1,\ldots,p_n}$. Here, we give the perturbative expansion up to order 10 of E_0 and the $\tilde{C}$'s in the limiting case $J_x, J_y \ll J_z$. Setting $J_z = 1/2$, one gets the following results.

(i) Constant term,

TABLE II. Operators appearing in Ω_{eff} with the corresponding coefficient up to order 2.

Order	Operator	Coefficient
1	$T_{-2}\Omega$	$-1/2$
1	$T_{+2}\Omega$	1/2
1	ΩT_{-2}	1/2
1	ΩT_{+2}	$-1/2$
2	$T_{-2}T_{-2}\Omega$	1/8
2	$T_{-2}T_0\Omega$	1/4
2	$T_{-2}T_{+2}\Omega$	$-1/8$
2	$T_{-2}\Omega T_{-2}$	$-1/4$
2	$T_{-2}\Omega T_{+2}$	1/4
2	$T_0T_{-2}\Omega$	$-1/4$
2	$T_0T_{+2}\Omega$	$-1/4$
2	$T_{+2}T_{-2}\Omega$	$-1/8$
2	$T_{+2}T_0\Omega$	1/4
2	$T_{+2}T_{+2}\Omega$	1/8
2	$T_{+2}\Omega T_{-2}$	1/4
2	$T_{+2}\Omega T_{+2}$	$-1/4$
2	$\Omega T_{-2}T_{-2}$	1/8
2	$\Omega T_{-2}T_0$	$-1/4$
2	$\Omega T_{-2}T_{+2}$	$-1/8$
2	ΩT_0T_{-2}	1/4
2	ΩT_0T_{+2}	1/4
2	$\Omega T_{+2}T_{-2}$	$-1/8$
2	$\Omega T_{+2}T_0$	$-1/4$
2	$\Omega T_{+2}T_{+2}$	1/8

$$\frac{E_0}{N} = -\frac{1}{2} - \frac{J_x^2+J_y^2}{2} - \frac{J_x^4+J_y^4}{8} - \frac{J_x^6+J_y^6}{8} - \frac{25}{128}(J_x^8+J_y^8) + \frac{9}{32}J_x^4J_y^4 - \frac{49}{128}(J_x^{10}+J_y^{10}) + \frac{33}{64}(J_x^6J_y^4+J_x^4J_y^6), \tag{C2}$$

where N is the number of z dimmers.

(ii) One-plaquette term,

$$C_p = \frac{1}{2}J_x^2J_y^2 + \frac{1}{4}(J_x^4J_y^2+J_x^2J_y^4) + \frac{5}{16}(J_x^6J_y^2+J_x^2J_y^6) + \frac{1}{4}J_x^4J_y^4 + \frac{35}{64}(J_x^8J_y^2+J_x^2J_y^8) - \frac{59}{32}(J_x^6J_y^4+J_x^4J_y^6).$$

(iii) Two-plaquette terms,

$$\tilde{C}_{\boldsymbol{n}_1} = \frac{7}{8}J_x^4J_y^2 - \frac{15}{16}J_x^4J_y^4 + \frac{3}{4}J_x^6J_y^2 + \frac{77}{64}J_x^8J_y^2 - \frac{55}{32}J_x^6J_y^4 - \frac{297}{128}J_x^4J_y^6,$$

$$\tilde{C}_{\boldsymbol{n}_2} = \frac{7}{8}J_x^2J_y^4 - \frac{15}{16}J_x^4J_y^4 + \frac{3}{4}J_x^2J_y^6 + \frac{77}{64}J_x^2J_y^8 - \frac{55}{32}J_x^4J_y^6 - \frac{297}{128}J_x^6J_y^4,$$

$$\tilde{C}_{\boldsymbol{n}_1+\boldsymbol{n}_2} = \frac{33}{8}J_x^4J_y^4,$$

$$\tilde{C}_{\boldsymbol{n}_1-\boldsymbol{n}_2} = -\frac{1}{4}J_x^4J_y^4 - \frac{3}{32}(J_x^6J_y^4 + J_x^4J_y^6),$$

$$\tilde{C}_{2\boldsymbol{n}_1} = -\frac{143}{32}J_x^6J_y^4,$$

$$\tilde{C}_{2\boldsymbol{n}_2} = -\frac{143}{32}J_x^4J_y^6,$$

$$\tilde{C}_{2\boldsymbol{n}_1+\boldsymbol{n}_2} = \frac{715}{64}J_x^6J_y^4,$$

$$\tilde{C}_{2\boldsymbol{n}_1-\boldsymbol{n}_2} = \frac{55}{64}J_x^6J_y^4,$$

$$\tilde{C}_{\boldsymbol{n}_1+2\boldsymbol{n}_2} = \frac{715}{64}J_x^4J_y^6,$$

$$\tilde{C}_{-\boldsymbol{n}_1+2\boldsymbol{n}_2} = \frac{55}{64}J_x^4J_y^6.$$

(iv) Three-plaquette terms,

$$\tilde{C}_{\boldsymbol{n}_1,2\boldsymbol{n}_1} = \frac{33}{16}J_x^6J_y^2 - \frac{143}{32}J_x^6J_y^4 + \frac{143}{64}J_x^8J_y^2,$$

$$\tilde{C}_{\boldsymbol{n}_2,2\boldsymbol{n}_2} = \frac{33}{16}J_x^2J_y^6 - \frac{143}{32}J_x^4J_y^6 + \frac{143}{64}J_x^2J_y^8,$$

$$\tilde{C}_{\boldsymbol{n}_1,\boldsymbol{n}_1+\boldsymbol{n}_2} = \frac{33}{16}J_x^4J_y^4 - \frac{143}{128}(J_x^6J_y^4 + J_x^4J_y^6),$$

$$\tilde{C}_{\boldsymbol{n}_1,-\boldsymbol{n}_2} = \frac{33}{16}J_x^4J_y^4 - \frac{143}{128}(J_x^6J_y^4 + J_x^4J_y^6),$$

$$\tilde{C}_{\boldsymbol{n}_1,\boldsymbol{n}_1-\boldsymbol{n}_2} = -\frac{9}{16}J_x^4J_y^4 - \frac{275}{128}(J_x^6J_y^4 + J_x^4J_y^6),$$

$$\tilde{C}_{\boldsymbol{n}_1,\boldsymbol{n}_2} = -\frac{9}{16}J_x^4J_y^4 - \frac{275}{128}(J_x^6J_y^4 + J_x^4J_y^6),$$

$$\tilde{C}_{\boldsymbol{n}_1+\boldsymbol{n}_2,2\boldsymbol{n}_1+\boldsymbol{n}_2} = \frac{715}{64}J_x^6J_y^4,$$

$$\tilde{C}_{\boldsymbol{n}_1+\boldsymbol{n}_2,\boldsymbol{n}_1+2\boldsymbol{n}_2} = \frac{715}{64}J_x^4J_y^6,$$

$$\tilde{C}_{\boldsymbol{n}_1,2\boldsymbol{n}_1+\boldsymbol{n}_2} = \frac{715}{64}J_x^6J_y^4,$$

$$\tilde{C}_{\boldsymbol{n}_2,\boldsymbol{n}_1+2\boldsymbol{n}_2} = \frac{715}{64}J_x^4J_y^6,$$

$$\tilde{C}_{\boldsymbol{n}_1-\boldsymbol{n}_2,2\boldsymbol{n}_1-\boldsymbol{n}_2} = -\frac{11}{16}J_x^6J_y^4,$$

$$\tilde{C}_{\boldsymbol{n}_1-\boldsymbol{n}_2,\boldsymbol{n}_1-2\boldsymbol{n}_2} = -\frac{11}{16}J_x^4J_y^6,$$

$$\tilde{C}_{\boldsymbol{n}_1,2\boldsymbol{n}_1-\boldsymbol{n}_2} = -\frac{11}{16}J_x^6J_y^4,$$

$$\tilde{C}_{\boldsymbol{n}_2,\boldsymbol{n}_1-\boldsymbol{n}_2} = -\frac{11}{16}J_x^4J_y^6.$$

(v) Four-plaquette terms,

$$\tilde{C}_{\boldsymbol{n}_1,\boldsymbol{n}_2,\boldsymbol{n}_1+\boldsymbol{n}_2} = \frac{33}{16}J_x^4J_y^4,$$

$$\tilde{C}_{\boldsymbol{n}_1,\boldsymbol{n}_2,-\boldsymbol{n}_1+\boldsymbol{n}_2} = \frac{55}{128}J_x^6J_y^4,$$

$$\tilde{C}_{\boldsymbol{n}_1,\boldsymbol{n}_2,\boldsymbol{n}_1-\boldsymbol{n}_2} = \frac{55}{128}J_x^4J_y^6,$$

$$\tilde{C}_{\boldsymbol{n}_1,2\boldsymbol{n}_1,3\boldsymbol{n}_1} = \frac{715}{128}J_x^8J_y^2,$$

$$\tilde{C}_{\boldsymbol{n}_2,2\boldsymbol{n}_2,3\boldsymbol{n}_2} = \frac{715}{128}J_x^2J_y^8,$$

$$\tilde{C}_{\boldsymbol{n}_1,\boldsymbol{n}_1+\boldsymbol{n}_2,\boldsymbol{n}_1+2\boldsymbol{n}_2} = \frac{715}{128}J_x^4J_y^6,$$

$$\tilde{C}_{\boldsymbol{n}_2,\boldsymbol{n}_1+\boldsymbol{n}_2,2\boldsymbol{n}_1+\boldsymbol{n}_2} = \frac{715}{128}J_x^6J_y^4,$$

$$\tilde{C}_{\boldsymbol{n}_1,2\boldsymbol{n}_1,2\boldsymbol{n}_1+\boldsymbol{n}_2} = \frac{715}{128}J_x^6J_y^4,$$

$$\tilde{C}_{\boldsymbol{n}_2,2\boldsymbol{n}_2,\boldsymbol{n}_1+2\boldsymbol{n}_2} = \frac{715}{128}J_x^4J_y^6,$$

$$\tilde{C}_{\boldsymbol{n}_1,\boldsymbol{n}_1+\boldsymbol{n}_2,2\boldsymbol{n}_1+\boldsymbol{n}_2} = \frac{715}{128}J_x^6J_y^4,$$

$$\tilde{C}_{\boldsymbol{n}_2,\boldsymbol{n}_1+\boldsymbol{n}_2,\boldsymbol{n}_1+2\boldsymbol{n}_2} = \frac{715}{128}J_x^4J_y^6,$$

$$\tilde{C}_{\boldsymbol{n}_1,2\boldsymbol{n}_1,\boldsymbol{n}_2} = -\frac{143}{128}J_x^6J_y^4,$$

$$\tilde{C}_{\boldsymbol{n}_2,2\boldsymbol{n}_2,\boldsymbol{n}_1} = -\frac{143}{128}J_x^4J_y^6,$$

$$\tilde{C}_{\boldsymbol{n}_1,2\boldsymbol{n}_1,2\boldsymbol{n}_1-\boldsymbol{n}_2} = -\frac{143}{128}J_x^6J_y^4,$$

$$\tilde{C}_{\boldsymbol{n}_1,\boldsymbol{n}_1-\boldsymbol{n}_2,\boldsymbol{n}_1-2\boldsymbol{n}_2} = -\frac{143}{128}J_x^4J_y^6,$$

$$\tilde{C}_{\boldsymbol{n}_1,\boldsymbol{n}_1+\boldsymbol{n}_2,2\boldsymbol{n}_1} = -\frac{143}{128}J_x^6 J_y^4,$$

$$\tilde{C}_{\boldsymbol{n}_1,\boldsymbol{n}_1-\boldsymbol{n}_2,2\boldsymbol{n}_1} = -\frac{143}{128}J_x^6 J_y^4,$$

$$\tilde{C}_{\boldsymbol{n}_1,\boldsymbol{n}_2,-\boldsymbol{n}_1} = -\frac{143}{128}J_x^4 J_y^6,$$

$$\tilde{C}_{\boldsymbol{n}_1,\boldsymbol{n}_1+\boldsymbol{n}_2,\boldsymbol{n}_1-\boldsymbol{n}_2} = -\frac{143}{128}J_x^4 J_y^6.$$

(vi) Five-plaquette terms,

$$\tilde{C}_{\boldsymbol{n}_1,2\boldsymbol{n}_1,\boldsymbol{n}_1+\boldsymbol{n}_2,2\boldsymbol{n}_1+\boldsymbol{n}_2} = \frac{715}{128}J_x^6 J_y^4,$$

$$\tilde{C}_{\boldsymbol{n}_1,2\boldsymbol{n}_1,-\boldsymbol{n}_2,\boldsymbol{n}_1-\boldsymbol{n}_2} = \frac{715}{128}J_x^6 J_y^4,$$

$$\tilde{C}_{\boldsymbol{n}_2,2\boldsymbol{n}_2,\boldsymbol{n}_1+\boldsymbol{n}_2,\boldsymbol{n}_1+2\boldsymbol{n}_2} = \frac{715}{128}J_x^4 J_y^6,$$

$$\tilde{C}_{\boldsymbol{n}_2,2\boldsymbol{n}_2,-\boldsymbol{n}_1,-\boldsymbol{n}_1+\boldsymbol{n}_2} = \frac{715}{128}J_x^4 J_y^6,$$

$$\tilde{C}_{\boldsymbol{n}_1,2\boldsymbol{n}_1,\boldsymbol{n}_2,\boldsymbol{n}_1+\boldsymbol{n}_2} = -\frac{143}{128}J_x^6 J_y^4,$$

$$\tilde{C}_{\boldsymbol{n}_1,2\boldsymbol{n}_1,\boldsymbol{n}_1-\boldsymbol{n}_2,2\boldsymbol{n}_1-\boldsymbol{n}_2} = -\frac{143}{128}J_x^6 J_y^4,$$

$$\tilde{C}_{\boldsymbol{n}_2,2\boldsymbol{n}_2,\boldsymbol{n}_1,\boldsymbol{n}_1+\boldsymbol{n}_2} = -\frac{143}{128}J_x^4 J_y^6,$$

$$\tilde{C}_{\boldsymbol{n}_2,2\boldsymbol{n}_2,-\boldsymbol{n}_1+\boldsymbol{n}_2,-\boldsymbol{n}_1+2\boldsymbol{n}_2} = -\frac{143}{128}J_x^4 J_y^6.$$

(vii) Six-plaquette terms,

$$\tilde{C}_{\boldsymbol{n}_1,2\boldsymbol{n}_1,\boldsymbol{n}_2,\boldsymbol{n}_1+\boldsymbol{n}_2,2\boldsymbol{n}_1+\boldsymbol{n}_2} = \frac{715}{128}J_x^6 J_y^4,$$

$$\tilde{C}_{\boldsymbol{n}_2,2\boldsymbol{n}_2,\boldsymbol{n}_1,\boldsymbol{n}_1+\boldsymbol{n}_2,\boldsymbol{n}_1+2\boldsymbol{n}_2} = \frac{715}{128}J_x^4 J_y^6.$$

As can be seen from these expansions, the number of interacting plaquettes increases with the order of the perturbation theory.

APPENDIX D: COEFFICIENTS OF THE PERTURBATIVE EXPANSION OF THE HAMILTONIAN IN THE 1-QP SECTOR

In the 1-QP sector, the effective Hamiltonian reads [see Eqs. (26)–(30)]

$$H_{\text{eff}}|_{q=1} = H_{\text{eff}}|_{q=0} + \mu - \sum_{\{j_1,\ldots j_n\}} D_{j_1,\ldots,j_n} t_{j_{n-1}}^{j_n} \ldots t_{j_1}^{j_2}, \quad \text{(D1)}$$

where the sum is performed over all non-self-retracing paths of length n starting at site $\boldsymbol{j}_1$ and ending at site $\boldsymbol{j}_n$. The operators $t_{\boldsymbol{i}}^{\boldsymbol{j}}$ are defined in Eqs. (10)–(13). Since the D's do not depend on the initial site, we introduce $\tilde{D}_{j_2-j_1,\ldots j_n-j_{n-1}} = D_{j_1,\ldots j_n}$. From the symmetries of the underlying lattice, it is clear that we can limit the analysis to processes involving a first jump in the direction $+\boldsymbol{n}_1$ or $+\boldsymbol{n}_2$.

We give below the perturbative expansion of μ and the $\tilde{D}$'s in the limiting case $J_x, J_y \ll J_z$ up to order 4 and set $J_z = 1/2$. Note that one could reach order 10 as for the 0-QP sector if needed. However, as explained in Sec. VI, it is simpler, in this sector, to use directly the Majorana formalism, which is nonperturbative and requires a comparable numerical effort.

(i) Chemical potential,

$$\mu = 1 + J_x^2 + J_y^2 + \frac{J_x^4 + J_y^4}{4}. \quad \text{(D2)}$$

(ii) One-hopping terms,

$$\tilde{D}_{n_1} = J_x - \frac{1}{2}J_x^3 - \frac{1}{2}J_x J_y^2,$$

$$\tilde{D}_{n_2} = J_y - \frac{1}{2}J_y^3 - \frac{1}{2}J_x^2 J_y.$$

(iii) Two-hopping terms,

$$\tilde{D}_{n_1,n_1} = \frac{1}{2}J_x^2 - \frac{5}{8}J_x^2 J_y^2 - \frac{1}{2}J_x^4,$$

$$\tilde{D}_{n_1,n_2} = \frac{1}{2}J_x J_y - \frac{9}{16}J_x^3 J_y - \frac{9}{16}J_x J_y^3,$$

$$\tilde{D}_{n_1,-n_2} = -\frac{1}{2}J_x J_y,$$

$$\tilde{D}_{n_2,n_2} = \frac{1}{2}J_y^2 - \frac{5}{8}J_x^2 J_y^2 - \frac{1}{2}J_y^4,$$

$$\tilde{D}_{n_2,n_1} = \frac{1}{2}J_x J_y - \frac{9}{16}J_x J_y^3 - \frac{9}{16}J_x^3 J_y,$$

$$\tilde{D}_{n_2,-n_1} = -\frac{1}{2}J_x J_y.$$

(iv) Three-hopping terms,

$$\tilde{D}_{n_1,n_1,n_1} = \frac{1}{2}J_x^3,$$

$$\tilde{D}_{n_1,n_1,n_2} = \frac{1}{2}J_x^2 J_y,$$

$$\tilde{D}_{n_1,n_1,-n_2} = -\frac{1}{4}J_x^2 J_y,$$

$$\tilde{D}_{n_1,n_2,n_1} = \frac{1}{2}J_x^2 J_y,$$

$$\tilde{D}_{n_1,n_2,n_2} = \frac{1}{2}J_x J_y^2,$$

$$\tilde{D}_{n_1,n_2,-n_1} = -\frac{1}{4}J_x^2 J_y,$$

$$\tilde{D}_{n_1,-n_2,n_1} = 0,$$

$$\tilde{D}_{n_1,-n_2,-n_2} = -\frac{1}{4}J_x J_y^2,$$

$$\tilde{D}_{n_1,-n_2,-n_1} = -\frac{1}{4}J_x^2 J_y,$$

$$\tilde{D}_{n_2,n_2,n_2} = \frac{1}{2}J_y^3,$$

$$\tilde{D}_{n_2,n_2,n_1} = \frac{1}{2}J_x J_y^2,$$

$$\tilde{D}_{n_2,n_2,-n_1} = -\frac{1}{4}J_x J_y^2,$$

$$\tilde{D}_{n_2,n_1,n_2} = \frac{1}{2}J_x J_y^2,$$

$$\tilde{D}_{n_2,n_1,n_1} = \frac{1}{2}J_x^2 J_y,$$

$$\tilde{D}_{n_2,n_1,-n_2} = -\frac{1}{4}J_x J_y^2,$$

$$\tilde{D}_{n_2,-n_1,n_2} = 0,$$

$$\tilde{D}_{n_2,-n_1,-n_1} = -\frac{1}{4}J_x^2 J_y,$$

$$\tilde{D}_{n_2,-n_1,-n_2} = -\frac{1}{4}J_x J_y^2.$$

(v) Four-hopping terms,

$$\tilde{D}_{n_1,n_1,n_1,n_1} = \frac{5}{8}J_x^4,$$

$$\tilde{D}_{n_1,n_1,n_1,n_2} = \frac{5}{8}J_x^3 J_y,$$

$$\tilde{D}_{n_1,n_1,n_1,-n_2} = -\frac{3}{16}J_x^3 J_y,$$

$$\tilde{D}_{n_1,n_1,n_2,n_1} = \frac{5}{8}J_x^3 J_y,$$

$$\tilde{D}_{n_1,n_1,n_2,n_2} = \frac{5}{8}J_x^2 J_y^2,$$

$$\tilde{D}_{n_1,n_1,n_2,-n_1} = -\frac{3}{16}J_x^3 J_y,$$

$$\tilde{D}_{n_1,n_1,-n_2,n_1} = -\frac{1}{16}J_x^3 J_y,$$

$$\tilde{D}_{n_1,n_1,-n_2,-n_2} = -\frac{1}{4}J_x^2 J_y^2,$$

$$\tilde{D}_{n_1,n_1,-n_2,-n_1} = -\frac{1}{4}J_x^3 J_y,$$

$$\tilde{D}_{n_1,n_2,n_1,n_1} = \frac{5}{8}J_x^3 J_y,$$

$$\tilde{D}_{n_1,n_2,n_1,n_2} = \frac{5}{8}J_x^2 J_y^2,$$

$$\tilde{D}_{n_1,n_2,n_1,-n_2} = -\frac{3}{16}J_x^2 J_y^2,$$

$$\tilde{D}_{n_1,n_2,n_2,n_1} = \frac{5}{8}J_x^2 J_y^2,$$

$$\tilde{D}_{n_1,n_2,n_2,n_2} = \frac{5}{8}J_x J_y^3,$$

$$\tilde{D}_{n_1,n_2,n_2,-n_1} = -\frac{3}{16}J_x^2 J_y^2,$$

$$\tilde{D}_{n_1,n_2,-n_1,-n_1} = -\frac{1}{4}J_x^3 J_y,$$

$$\tilde{D}_{n_1,n_2,-n_1,n_2} = -\frac{1}{16}J_x^2 J_y^2,$$

$$\tilde{D}_{n_1,-n_2,n_1,n_1} = -\frac{1}{16}J_x^3 J_y,$$

$$\tilde{D}_{n_1,-n_2,n_1,n_2} = -\frac{1}{16}J_x^2 J_y^2,$$

$$\tilde{D}_{n_1,-n_2,n_1,-n_2} = \frac{1}{8}J_x^2 J_y^2,$$

$$\tilde{D}_{n_1,-n_2,-n_2,n_1} = 0,$$

$$\tilde{D}_{n_1,-n_2,-n_2,-n_2} = -\frac{3}{16} J_x J_y^3,$$

$$\tilde{D}_{n_1,-n_2,-n_2,-n_1} = -\frac{3}{16} J_x^2 J_y^2,$$

$$\tilde{D}_{n_1,-n_2,-n_1,-n_1} = -\frac{3}{16} J_x^3 J_y,$$

$$\tilde{D}_{n_1,-n_2,-n_1,-n_2} = -\frac{3}{16} J_x^2 J_y^2,$$

$$\tilde{D}_{n_2,n_2,n_2,n_2} = \frac{5}{8} J_y^4,$$

$$\tilde{D}_{n_2,n_2,n_2,n_1} = \frac{5}{8} J_x J_y^3,$$

$$\tilde{D}_{n_2,n_2,n_2,-n_1} = -\frac{3}{16} J_x J_y^3,$$

$$\tilde{D}_{n_2,n_2,n_1,n_2} = \frac{5}{8} J_x J_y^3,$$

$$\tilde{D}_{n_2,n_2,n_1,n_1} = \frac{5}{8} J_x^2 J_y^2,$$

$$\tilde{D}_{n_2,n_2,n_1,-n_2} = -\frac{3}{16} J_x J_y^3,$$

$$\tilde{D}_{n_2,n_2,-n_1,n_2} = -\frac{1}{16} J_x J_y^3,$$

$$\tilde{D}_{n_2,n_2,-n_1,-n_1} = -\frac{1}{4} J_x^2 J_y^2,$$

$$\tilde{D}_{n_2,n_2,-n_1,-n_2} = -\frac{1}{4} J_x J_y^3,$$

$$\tilde{D}_{n_2,n_1,n_2,n_2} = \frac{5}{8} J_x J_y^3,$$

$$\tilde{D}_{n_2,n_1,n_2,n_1} = \frac{5}{8} J_x^2 J_y^2,$$

$$\tilde{D}_{n_2,n_1,n_2,-n_1} = -\frac{3}{16} J_x^2 J_y^2,$$

$$\tilde{D}_{n_2,n_1,n_1,n_2} = \frac{5}{8} J_x^2 J_y^2,$$

$$\tilde{D}_{n_2,n_1,n_1,n_1} = \frac{5}{8} J_x^3 J_y,$$

$$\tilde{D}_{n_2,n_1,n_1,-n_2} = -\frac{3}{16} J_x^2 J_y^2,$$

$$\tilde{D}_{n_2,n_1,-n_2,-n_2} = -\frac{1}{4} J_x J_y^3,$$

$$\tilde{D}_{n_2,n_1,-n_2,n_1} = -\frac{1}{16} J_y^2 J_y^2,$$

$$\tilde{D}_{n_2,-n_1,n_2,n_2} = -\frac{1}{16} J_x J_y^3,$$

$$\tilde{D}_{n_2,-n_1,n_2,n_1} = -\frac{1}{16} J_x^2 J_y^2,$$

$$\tilde{D}_{n_2,-n_1,n_2,-n_1} = \frac{1}{8} J_x^2 J_y^2,$$

$$\tilde{D}_{n_2,-n_1,-n_1,n_2} = 0,$$

$$\tilde{D}_{n_2,-n_1,-n_1,-n_1} = -\frac{3}{16} J_x^3 J_y,$$

$$\tilde{D}_{n_2,-n_1,-n_1,-n_2} = -\frac{3}{16} J_x^2 J_y^2,$$

$$\tilde{D}_{n_2,-n_1,-n_2,-n_2} = -\frac{3}{16} J_x J_y^3,$$

$$\tilde{D}_{n_2,-n_1,-n_2,-n_1} = -\frac{3}{16} J_x^2 J_y^2.$$

Additionally, there are some terms corresponding to processes where the particle hops one time around a plaquette. Note that the plaquette involved can be covered clockwise or counterclockwise but the product of t_i^j leads exactly to the same operator $b_i^\dagger b_i W_p$,

$$\tilde{D}_{n_1,-n_2,-n_1,n_2} = \frac{1}{4} J_x^2 J_y^2,$$

$$\tilde{D}_{n_1,n_2,-n_1,-n_2} = 0,$$

$$\tilde{D}_{n_2,-n_1,-n_2,n_1} = \frac{1}{4} J_x^2 J_y^2,$$

$$\tilde{D}_{n_2,n_1,-n_2,-n_1} = 0.$$

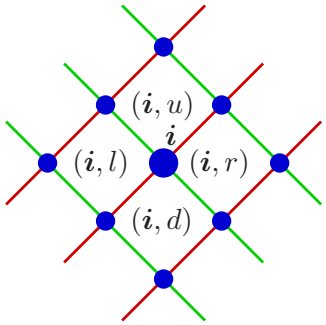

FIG. 25. (Color online) Labeling of the plaquettes by a site index ($\boldsymbol{i}$) and a position u,d,l,r with respect to that site.

APPENDIX E: COEFFICIENTS OF THE SPIN-SPIN CORRELATION FUNCTION IN THE 0-QP SECTOR

As discussed in Sec. IX A, the spin-spin correlation functions $C_{ij}^{\alpha\beta}=\sigma_i^\alpha\sigma_j^\beta$ computed on any eigenstate of H are nonvanishing only if $\alpha=\beta$ and if $\boldsymbol{i}$ and $\boldsymbol{j}$ belong to the same dimer which is of α type. We give below the perturbative expansion of these correlation functions in the 0-QP sector.

1. Coefficients of C_i^{zz}

In the perturbative approach we use, note that a z dimer in the honeycomb lattice becomes a single site $\boldsymbol{i}$ in the effective square lattice. As for the Hamiltonian in the 0-QP sector [see Eq. (21)], we obtain an expansion which can be expressed only in terms of the plaquette operators, namely,

$$C_{\boldsymbol{i}}^{zz}|_{q=0}=a^{zz}-\sum_{\{p_1,\ldots,p_n\}}b^{zz}_{p_1,\ldots,p_n}W_{p_1}\cdots W_{p_n}. \tag{E1}$$

Below, we give the results up to order 6 and we index a plaquette p by a site $\boldsymbol{i}$ and indices u,d,l,r according to notations given in Fig. 25.

(i) Constant term,

$$a^{zz}=1-(J_x^2+J_y^2)-\frac{3}{4}(J_x^4+J_y^4)-\frac{5}{4}(J_x^6+J_y^6).$$

(ii) One-plaquette terms,

$$b^{zz}_{(\boldsymbol{i},u)}=-\frac{5}{4}J_x^2J_y^2,$$

$$b^{zz}_{(\boldsymbol{i},d)}=-\frac{5}{4}J_x^2J_y^2,$$

$$b^{zz}_{(\boldsymbol{i},l)}=-\frac{1}{4}J_x^2J_y^2+\frac{1}{2}(J_x^2J_y^4+J_x^4J_y^2),$$

$$b^{zz}_{(\boldsymbol{i},r)}=-\frac{1}{4}J_x^2J_y^2+\frac{1}{2}(J_x^2J_y^4+J_x^4J_y^2),$$

$$b^{zz}_{(\boldsymbol{i}+2\boldsymbol{n}_1,l)}=-\frac{21}{8}J_x^4J_y^2,$$

$$b^{zz}_{(\boldsymbol{i}+2\boldsymbol{n}_2,r)}=-\frac{21}{8}J_x^2J_y^4,$$

$$b^{zz}_{(\boldsymbol{i}-2\boldsymbol{n}_1,r)}=-\frac{21}{8}J_x^4J_y^2,$$

$$b^{zz}_{(\boldsymbol{i}-2\boldsymbol{n}_2,l)}=-\frac{21}{8}J_x^2J_y^4,$$

$$b^{zz}_{(\boldsymbol{i}-2\boldsymbol{n}_1,u)}=\frac{7}{8}J_x^4J_y^2,$$

$$b^{zz}_{(\boldsymbol{i}+2\boldsymbol{n}_2,d)}=\frac{7}{8}J_x^2J_y^4,$$

$$b^{zz}_{(\boldsymbol{i}+2\boldsymbol{n}_1,d)}=\frac{7}{8}J_x^4J_y^2,$$

$$b^{zz}_{(\boldsymbol{i}-2\boldsymbol{n}_2,u)}=\frac{7}{8}J_x^2J_y^4. \tag{E2}$$

(iii) Two-plaquette terms,

$$b^{zz}_{(\boldsymbol{i},u),(\boldsymbol{i}+2\boldsymbol{n}_1,l)}=-\frac{21}{8}J_x^4J_y^2,$$

$$b^{zz}_{(\boldsymbol{i},u),(\boldsymbol{i}+2\boldsymbol{n}_2,r)}=-\frac{21}{8}J_x^2J_y^4,$$

$$b^{zz}_{(\boldsymbol{i},d),(\boldsymbol{i}-2\boldsymbol{n}_1,r)}=-\frac{21}{8}J_x^4J_y^2,$$

$$b^{zz}_{(\boldsymbol{i},d),(\boldsymbol{i}-2\boldsymbol{n}_2,l)}=-\frac{21}{8}J_x^2J_y^4,$$

$$b^{zz}_{(\boldsymbol{i},l),(\boldsymbol{i}-2\boldsymbol{n}_1,u)}=-\frac{7}{8}J_x^4J_y^2,$$

$$b^{zz}_{(\boldsymbol{i},l),(\boldsymbol{i}+2\boldsymbol{n}_2,d)}=-\frac{7}{8}J_x^2J_y^4,$$

$$b^{zz}_{(\boldsymbol{i},r),(\boldsymbol{i}+2\boldsymbol{n}_1,d)}=-\frac{7}{8}J_x^4J_y^2,$$

$$b^{zz}_{(\boldsymbol{i},r),(\boldsymbol{i}-2\boldsymbol{n}_2,u)}=-\frac{7}{8}J_x^2J_y^4,$$

$$b^{zz}_{(\boldsymbol{i},u),(\boldsymbol{i},l)}=-\frac{7}{8}J_x^4J_y^2,$$

$$b^{zz}_{(\boldsymbol{i},d),(\boldsymbol{i},l)}=-\frac{7}{8}J_x^2J_y^4,$$

$$b^{zz}_{(\boldsymbol{i},d),(\boldsymbol{i},r)}=-\frac{7}{8}J_x^4J_y^2,$$

$$b^{zz}_{(\boldsymbol{i},u),(\boldsymbol{i},r)} = -\frac{7}{8}J_x^2 J_y^4.$$

2. Coefficients of $C^{xx}_{\boldsymbol{i},\boldsymbol{j}}$

Contrary to z dimers, x dimers remain dimers perturbatively. Here again, one obtains an expansion in terms of plaquettes for these observables, in the 0-QP sector, which can be written as

$$C^{xx}_{\boldsymbol{i},\boldsymbol{i}+\boldsymbol{n}_1}|_{q=0} = a^{xx} - \sum_{\{p_1,\ldots,p_n\}} b^{xx}_{p_1,\ldots,p_n} W_{p_1}\cdots W_{p_n}. \quad \text{(E3)}$$

We give below the expansion of the coefficients up to order 5 (only odd orders are nonvanishing), and, as previously, we index a plaquette p by a site $\boldsymbol{i}$ and an index u,d,l,r according to the notations given in Fig. 25. In the following we consider a dimer located at $(\boldsymbol{i},\boldsymbol{i}+\boldsymbol{n}_1)$.

(i) Constant term,

$$a^{xx} = J_x + \frac{1}{2}J_x^3 + \frac{3}{4}J_x^5.$$

(ii) One-plaquette terms,

$$b^{xx}_{(\boldsymbol{i},u)} = \frac{1}{2}J_x J_y^2 - \frac{1}{2}J_x^3 J_y^2 + \frac{1}{4}J_x J_y^4,$$

$$b^{xx}_{(\boldsymbol{i},r)} = \frac{1}{2}J_x J_y^2 - \frac{1}{2}J_x^3 J_y^2 + \frac{1}{4}J_x J_y^4,$$

$$b^{xx}_{(\boldsymbol{i}+2\boldsymbol{n}_1,l)} = \frac{7}{4}J_x^3 J_y^2,$$

$$b^{xx}_{(\boldsymbol{i},d)} = \frac{7}{4}J_x^3 J_y^2,$$

$$b^{xx}_{(\boldsymbol{i}+2\boldsymbol{n}_1,d)} = -\frac{3}{4}J_x^3 J_y^2,$$

$$b^{xx}_{(\boldsymbol{i},l)} = -\frac{3}{4}J_x^3 J_y^2.$$

(iii) Two-plaquette terms,

$$b^{xx}_{(\boldsymbol{i},u),(\boldsymbol{i}+2\boldsymbol{n}_1,l)} = \frac{7}{8}J_x^3 J_y^2,$$

$$b^{xx}_{(\boldsymbol{i},u),(\boldsymbol{i}+2\boldsymbol{n}_2,r)} = \frac{7}{8}J_x J_y^4,$$

$$b^{xx}_{(\boldsymbol{i},u),(\boldsymbol{i},l)} = \frac{7}{8}J_x^3 J_y^2,$$

$$b^{xx}_{(\boldsymbol{i},r),(\boldsymbol{i},d)} = \frac{7}{8}J_x^3 J_y^2,$$

$$b^{xx}_{(\boldsymbol{i},r),(\boldsymbol{i}-2\boldsymbol{n}_2,u)} = \frac{7}{8}J_x J_y^4,$$

$$b^{xx}_{(\boldsymbol{i},r)(\boldsymbol{i}+2\boldsymbol{n}_1,d)} = \frac{7}{8}J_x^3 J_y^2. \quad \text{(E4)}$$

3. Coefficients of $C^{yy}_{\boldsymbol{i},\boldsymbol{j}}$

The correlation functions $C^{yy}_{\boldsymbol{i},\boldsymbol{j}}$ are straightforwardly obtained from $C^{xx}_{\boldsymbol{i},\boldsymbol{j}}$ by exchanging directions x and y as well as J_x and J_y.

APPENDIX F: CORRESPONDENCE BETWEEN THE MAJORANA FERMION SPECTRUM AND A FREE-PARTICLE PROBLEM IN A MAGNETIC FIELD

As shown by Kitaev,[7] the spin Hamiltonian (1) can be mapped onto the following Majorana fermion Hamiltonian,

$$H = \frac{\mathrm{i}}{4}\sum_{j,k} A_{jk}c_j c_k, \quad \text{(F1)}$$

where A is a skew-symmetric matrix of size $2N\times 2N$ (N being the number of plaquette) and where the c_j's are the (Hermitian) Majorana operators which obey $c_j^2=1$ and $c_j c_k=-c_k c_j$ if $j\neq k$. The sum is performed over all sites j and k of the honeycomb (brick-wall) lattice and

$$A_{jk} = 2J_\alpha u_{jk} \quad \text{(F2)}$$

if the link (j,k) is of α type and 0 otherwise. The u_{jk}'s are antisymmetric ($u_{jk}=-u_{kj}$) and take the values ± 1. These numbers define the vortex configuration through $w_p=\Pi_{(j,k)\in p}u_{jk}$, where j belongs to the black sublattice and k to the white one [see Fig. 1(a)]. We refer the interested reader to Ref. 7 for details. In the very end, the whole spectrum of H can be obtained once one knows the spectrum of iA, e.g., the ground-state energy per plaquette is given by

$$e_0 = -\frac{1}{4N}\mathrm{Tr}|\mathrm{i}A|. \quad \text{(F3)}$$

For a bipartite lattice such as the honeycomb lattice, we shall now show that the spectrum of iA is the same as the one-particle spectrum of the following Hamiltonian:

$$H' = -\frac{1}{2}\sum_{j,k} A'_{jk}(a_j^\dagger a_k + \mathrm{H.c.}), \quad \text{(F4)}$$

where $a_j^\dagger$ (a_j) are standard spinless fermion creation (annihilation) operators. The Hamiltonian H' describes free spinless fermions hopping in a honeycomb lattice in a magnetic field with a flux per plaquette which equals zero ($w_p=+1$) or half a flux quantum ($w_p=-1$). The spectra of H' (with one fermion) and of iA are identical provided

$$A'_{jk} = 2J_\alpha u'_{jk}, \quad \text{(F5)}$$

with $u'_{jk}=+u'_{kj}$. The choice of the u'_{jk} is as previously dictated by the flux configuration via $w_p=\Pi_{(j,k)\in p}u'_{jk}$, where, in this case, the u'_{jk} are not oriented but still take the value ± 1.

To show this, consider an eigenstate $|\psi\rangle$ of the matrix iA with energy E and let us denote $\psi_j=\langle j|\psi\rangle$ its component on site j. This state satisfies

$$\sum_k \mathrm{i}A_{jk}\psi_k = E\psi_j. \tag{F6}$$

Since the honeycomb lattice is bipartite, we can always set $u_{jk}=u'_{jk}$ if j is a white site (and k black) and $u_{jk}=-u'_{jk}$ if j is a black site (and k white). Then, one can easily check that the state $|\phi\rangle$, defined by $\phi_j=-\psi_j$ if j is a black site and $\phi_j=-\mathrm{i}\psi_j$ if it is a white site, satisfies

$$-\sum_k A'_{jk}\phi_k = E\phi_j, \tag{F7}$$

so that $|\phi\rangle$ is an eigenstate of H' with the energy E. This shows that H' (with one particle) and iA are isospectral. We insist on the fact that *this correspondence only holds for a bipartite lattice* but is no longer true in the presence of odd cycles.

*vidal@lptmc.jussieu.fr
†schmidt@fkt.physik.uni-dortmund.de
‡sdusuel@gmail.com

[1] J. M. Leinaas and J. Myrheim, Nuovo Cimento Soc. Ital. Fis., B **37**, 1 (1977).
[2] F. Wilczek, Phys. Rev. Lett. **48**, 1144 (1982).
[3] F. Wilczek, Phys. Rev. Lett. **49**, 957 (1982).
[4] D. E. Feldman, Y. Gefen, A. Kitaev, K. T. Law, and A. Stern, Phys. Rev. B **76**, 085333 (2007).
[5] http://www.theory.caltech.edu/people/preskill/ph229/
[6] A. Y. Kitaev, Ann. Phys. (N.Y.) **303**, 2 (2003).
[7] A. Kitaev, Ann. Phys. (N.Y.) **321**, 2 (2006).
[8] J. K. Pachos, Ann. Phys. (N.Y.) **322**, 1254 (2007).
[9] X.-Y. Feng, G.-M. Zhang, and T. Xiang, Phys. Rev. Lett. **98**, 087204 (2007).
[10] D.-H. Lee, G.-M. Zhang, and T. Xiang, Phys. Rev. Lett. **99**, 196805 (2007).
[11] H.-D. Chen and J. Hu, Phys. Rev. B **76**, 193101 (2007).
[12] H.-D. Chen and Z. Nussinov, J. Phys. A **41**, 075001 (2008).
[13] K. P. Schmidt, S. Dusuel, and J. Vidal, Phys. Rev. Lett. **100**, 057208 (2008).
[14] V. Lahtinen, G. Kells, A. Carollo, T. Stitt, J. Vala, and J. K. Pachos, Ann. Phys. (N.Y.) **323**, 2286 (2008).
[15] G. Kells, A. T. Bolukbasi, V. Lahtinen, J. K. Slingerland, J. K. Pachos, and J. Vala, arXiv:0804.2753, Phys. Rev. Lett. (to be published).
[16] S. Dusuel, K. P. Schmidt, and J. Vidal, Phys. Rev. Lett. **100**, 177204 (2008).
[17] G. Baskaran, S. Mandal, and R. Shankar, Phys. Rev. Lett. **98**, 247201 (2007).
[18] S. Yang, S.-J. Gu, C.-P. Sun, and H.-Q. Lin, Phys. Rev. A **78**, 012304 (2008).
[19] J.-H. Zhao and H.-Q. Zhou, arXiv:0803.0814 (unpublished).
[20] S.-J. Gu and H.-Q. Lin, arXiv:0807.3491 (unpublished).
[21] K. Sengupta, D. Sen, and S. Mondal, Phys. Rev. Lett. **100**, 077204 (2008).
[22] S. Mondal, D. Sen, and K. Sengupta, Phys. Rev. B **78**, 045101 (2008).
[23] J. Yu, S.-P. Kou, and X.-G. Wen, arXiv:0709.2276 (unpublished).
[24] S. Yang, D. L. Zhou, and C. P. Sun, Phys. Rev. B **76**, 180404(R) (2007).
[25] S. Mandal and N. Surendran, arXiv:0801.0229 (unpublished).
[26] H. Yao and S. A. Kivelson, Phys. Rev. Lett. **99**, 247203 (2007).
[27] S. Dusuel, K. P. Schmidt, J. Vidal, and R. L. Zaffino, Phys. Rev. B **78**, 125102 (2008).
[28] L.-M. Duan, E. Demler, and M. D. Lukin, Phys. Rev. Lett. **91**, 090402 (2003).
[29] A. Micheli, G. K. Brennen, and P. Zoller, Nat. Phys. **2**, 341 (2006).
[30] L. Jiang, G. K. Brennen, A. V. Gorshkov, K. Hammerer, M. Hafezi, E. Demler, M. D. Lukin, and P. Zoller, Nat. Phys. **4**, 482 (2008).
[31] M. Aguado, G. K. Brennen, F. Verstraete, and J. I. Cirac, arXiv:0802.3163 (unpublished).
[32] J. Q. You, X.-F. Shi, and F. Nori, arXiv:0809.0051 (unpublished).
[33] J. Vidal, S. Dusuel, and K. P. Schmidt, arXiv:0801.4620 (unpublished).
[34] F. Wegner, Ann. Phys. **3**, 77 (1994).
[35] S. D. Głazek and K. G. Wilson, Phys. Rev. D **48**, 5863 (1993).
[36] S. D. Głazek and K. G. Wilson, Phys. Rev. D **49**, 4214 (1994).
[37] S. Dusuel and G. S. Uhrig, J. Phys. A **37**, 9275 (2004).
[38] J. Stein, J. Stat. Phys. **88**, 487 (1997).
[39] C. Knetter and G. S. Uhrig, Eur. Phys. J. B **13**, 209 (2000).
[40] A. Mielke, Eur. Phys. J. B **5**, 605 (1998).
[41] X.-G. Wen, Phys. Rev. Lett. **90**, 016803 (2003).
[42] M. Levin and X.-G. Wen, Phys. Rev. B **67**, 245316 (2003).
[43] R. Rammal, J. Phys. (Paris) **46**, 1345 (1985).
[44] E. H. Lieb, Phys. Rev. Lett. **73**, 2158 (1994).
[45] C. Knetter, K. P. Schmidt, and G. S. Uhrig, Eur. Phys. J. B **36**, 525 (2004).
[46] C. Zhang, V. W. Scarola, S. Tewari, and S. Das Sarma, arXiv:0801.4918 (unpublished).
[47] I. S. Tupitsyn, A. Kitaev, N. V. Prokof'ev, and P. C. E. Stamp, arXiv:0804.3175 (unpublished).
[48] J. Vidal, S. Dusuel, and K. P. Schmidt, arXiv:0807.0487 (unpublished).
[49] http://t1.physik.uni-dortmund.de/uhrig/suppl.html